Journal of General Virology (2013), 94, 933–943 DOI 10.1099/vir.0.047167-0

Impact of antiretroviral pressure on selection of primary human immunodeficiency virus type 1 envelope sequences *in vitro*

Shigeyoshi Harada,[1,2] Kazuhisa Yoshimura,[1,2] Aki Yamaguchi,[1] Samatchaya Boonchawalit,[1,2] Keisuke Yusa[3] and Shuzo Matsushita[1]

Correspondence
Kazuhisa Yoshimura
ykazu@nih.go.jp

[1]Center for AIDS Research, Kumamoto University, 2-2-1 Honjo, Chuo-ku, Kumamoto 860-0811, Japan

[2]AIDS Research Center, National Institute of Infectious Diseases, 1-23-1 Toyama, Shinjuku-ku, Tokyo 162-8640, Japan

[3]Division of Biological Chemistry and Biologicals, National Institute of Health Sciences, 1-18-1 Kami-youga, Setagaya-ku, Tokyo 158-8501, Japan

The initiation of drug therapy results in a reduction in the human immunodeficiency virus type 1 (HIV-1) population, which represents a potential genetic bottleneck. The effect of this drug-induced genetic bottleneck on the population dynamics of the envelope (Env) regions has been addressed in several *in vivo* studies. However, it is difficult to investigate the effect on the *env* gene of the genetic bottleneck induced not only by entry inhibitors but also by non-entry inhibitors, particularly *in vivo*. Therefore, this study used an *in vitro* selection system using unique bulk primary isolates established in the laboratory to observe the effects of the antiretroviral drug-induced bottleneck on the integrase and *env* genes. Env diversity was decreased significantly in one primary isolate [KP-1, harbouring both CXCR4 (X4)- and CCR5 (R5)-tropic variants] when passaged in the presence or absence of raltegravir (RAL) during *in vitro* selection. Furthermore, the RAL-selected KP-1 variant had a completely different Env sequence from that in the passage control (particularly evident in the gp120, V1/V2 and V4-loop regions), and a different number of potential *N*-glycosylation sites. A similar pattern was also observed in other primary isolates when using different classes of drugs. This is the first study to explore the influence of anti-HIV drugs on bottlenecks in bulk primary HIV isolates with highly diverse Env sequences using *in vitro* selection.

Received 15 August 2012
Accepted 20 December 2012

INTRODUCTION

Human immunodeficiency virus type 1 (HIV-1) shows a high degree of genetic diversity owing to its high rates of replication and recombination and the high mutation rate of the HIV-1 reverse transcriptase (Nájera *et al.*, 2002). Even in a single infected individual, the virus can best be described as a population of distinct, but closely related, genetic variants or 'quasi-species' (Eigen, 1993; Nijhuis *et al.*, 1998). The quasi-species behaviour of viruses is recognized as a key element in our understanding and modelling of viral evolution and disease control (Vignuzzi *et al.*, 2006).

The GenBank/EMBL/DDBJ accession numbers for the *env* sequences of HIV-1 KP-1, KP-2 and KP-4, are AB640872–AB640881, AB641341–AB641351 and AB641335–AB641340, respectively.

Two supplementary figures are available with the online version of this paper.

Combination antiretroviral (ARV) therapy results in a contraction of the viral population, which represents a potential genetic bottleneck (Charpentier *et al.*, 2006; Delwart *et al.*, 1998; Ibáñez *et al.*, 2000; Kitrinos *et al.*, 2005; Nijhuis *et al.*, 1998; Nora *et al.*, 2007; Sheehy *et al.*, 1996; Zhang *et al.*, 1994). Whilst this bottleneck has a direct effect on the region that is being targeted by the drugs (e.g. protease or reverse transcriptase), it also affects other regions of the viral genome. Indeed, the effect of the drug-induced genetic bottleneck on the population dynamics of the envelope (Env) regions has been addressed in several *in vivo* studies (Charpentier *et al.*, 2006; Delwart *et al.*, 1998; Ibáñez *et al.*, 2000; Kitrinos *et al.*, 2005; Nijhuis *et al.*, 1998; Nora *et al.*, 2007; Sheehy *et al.*, 1996; Zhang *et al.*, 1994).

Virus bottleneck evolution of the HIV-1 *env* gene might be important when choosing the optimal drugs to treat a particular patient. Indeed, a CCR5 antagonist (maraviroc, MVC) and a fusion inhibitor (enfuvirtide, T-20) have now

been approved for use as HIV-1 entry inhibitors. Analysing the dynamics of drug-induced genetic bottlenecks and studying drug-resistant mutation profiles in response to HIV-1-specific ARV drugs are both important if we are to understand fully HIV-1 drug resistance and pathogenesis.

The aim of the present study was to understand better the effect of *in vivo* drug-induced genetic bottlenecks. *In vitro* selection of different primary HIV-1 isolates was performed using the recently approved HIV integrase inhibitor raltegravir (RAL) (Steigbigel *et al.*, 2008). Two R5-, one X4-, one dual- and one mixed R5/X4-tropic isolates were passaged through a RAL-induced genetic bottleneck. We also performed *in vitro* selection of the R5/X4 isolate using lamivudine (3TC), saquinavir (SQV) and MVC, and compared the results with those from the RAL-selected isolate.

RESULTS

Genotypic profiles of the HIV-1 primary isolates

Four genetically heterogeneous HIV-1 primary isolates (KP-1–4) from Japanese drug-naïve patients were used to assess the extent to which RAL affected the selection of bulk primary viruses *in vitro*. A laboratory isolate, strain 89.6, was also used in the study (rather than a molecular clone) to allow escape mutants to be selected from each quasi-species pool and to be generated *de novo*. First, the sequences of the integrase (IN) regions of the four primary isolates were determined. Table 1 shows the detailed evaluation of the R5/X4 mixture subtype B (KP-1), R5-CRF08_BC (KP-2), R5 subtype B (KP-3) and X4-CRF01_AE (KP-4) primary isolates, and the dual-tropic subtype B laboratory virus (89.6). Although some naturally occurring polymorphisms were observed within the IN regions of these isolates compared with the subtype B consensus sequence available from the Los Alamos National Laboratory HIV sequence database, we did not identify any primary resistant mutations to RAL. Three baseline viruses (KP-1, KP-4 and 89.6) were sensitive to RAL, with IC_{50} values ranging from 1.2 to 4 nM, which are comparable with those reported previously (Kobayashi *et al.*, 2008). However, KP-2 and KP-3 showed minor resistance to RAL, with IC_{50} values of 16 and 32 nM, respectively. These two isolates contained amino acid mutations at positions 72, 125 and 201 within the IN region [previously reported as L-870,810 and S-1360 resistance mutations (Hombrouck *et al.*, 2008; Rhee *et al.*, 2008), but not as RAL-resistance mutations]. KP-2 also contained a unique insertion at position 288 (NQDME) at the C-terminal end of the IN region.

In vitro selection of variants of the primary isolates and 89.6 using RAL

To induce RAL-selected HIV-1 variants *in vitro*, PM1/CCR5 cells, a T-cell line expressing high levels of CCR5, were exposed to the four primary isolates and strain 89.6. The viruses were then serially passaged in the presence of RAL. As a control, each isolate was passaged under the same conditions, but without RAL, to allow monitoring of spontaneous changes occurring in the viruses during prolonged PM1/CCR5 cell passage (the passage control). The selected viruses were initially propagated at a RAL concentration equal to each IC_{50} value. The RAL concentrations were then increased from 20 to 85 nM during the course of the selection procedure (Table 1).

Only small shifts in the IC_{50} to RAL were observed in four of the five isolates (KP-1, KP-2, KP-4 and 89.6), with fold changes in IC_{50} values of 3.4, 6.5, 16 and 9.2, respectively. KP-3 did not show resistance to RAL. IC_{50} values in all the passage controls were comparable with those of the baseline viruses (Table 1).

IN region sequences in RAL-selected variants

The full-length *IN* genes were amplified and cloned to determine the genetic basis of selection in the presence or absence of RAL. Ten to 12 clones from each sample were sequenced.

Substitutions within IN were observed at passages 30 (G189R) and 29 (T210I) in two RAL-selected isolates (KP-2 and KP-4, respectively). Neither of these has been reported as IN inhibitor-resistant mutations. No substitutions in the IN regions of KP-3 and 89.6 were found. However, A125T and V180I substitutions were observed in the KP-3 and 89.6 control variants at the last passage. No previously reported mutations were identified in the IN region of KP-1 (an R5/X4 mixture isolate) after 17 passages. However, four amino acids (K7/K111/H216/D278) were selected by RAL from the baseline quasi-species, whereas different amino acids (R7/R111/Q216/N278) were selected in the control-passage variants (Table 1).

Taken together, these findings showed that RAL-induced selection pressure causes adaptation within the IN regions of bulk primary viruses during *in vitro* passage in the target cells, and confirmed that this system can be used to analyse drug-selected variants *in vitro*.

Comparison of *env* gene sequences in RAL-selected and passage-control isolates

A highly diverse gp120 region was observed in the baseline R5/X4 mixture isolate, KP-1; however, the viral diversity of variants passaged in the presence or absence of RAL decreased significantly during *in vitro* selection (overall mean distance after RAL selection of 0.056 at baseline to 0.007 after passage 17; mean overall distance in the passage control of 0.01 after 20 passages, Table 2). Moreover, the RAL-selected and control variants utilized CCR5 to enter the target cell; neither variant used CXCR4 (Table 3).

Interestingly, the low-diversity RAL-selected variant contained a completely different Env sequence from that of the passage-control variant (Fig. 1a). Different regions spanning

Table 1. Susceptibility of HIV-1 isolates to RAL and distinct differences in IN region sequences between RAL-selected and control-passaged viruses

Isolate	Subtype	Tropism	Passage no.	Concn (nM)	RAL-selected variant*		Passage control	
					IN sequence	RAL IC_{50} (nM)	IN sequence	RAL IC_{50} (nM)
KP-1	B	Mix	0	0	*K/R7, K/R111, Q/H216, D/N278*	4	*K/R7, K/R111, Q/H216, D/N278*	4
			8	20	**K**111, **H**216, **D**278	31 (7.8)	**R**7, **R**111, **Q**216, **N**278	4.5 (1.2)
			17†	20	**K**7, **K**111, **H**216, **D**278	26 (6.5)	**R**7, **R**111, **Q**216, **N**278	0.4 (0.1)
KP-2	CRF08_BC	R5	0	0	*I201, ins289NQDME*	16	*I201, ins289NQDME*	16
			18	40	G189G/R, *I201, ins289NQDME*	32 (2)	*I201, ins289NQDME*	16 (1)
			30	85	G189R, *I201, ins289NQDME*	55 (3.4)	*I201, ins289NQDME*	25 (1.6)
KP-3	B	R5	0	0	*V72, A125*	32	*V72, A125*	32
			11	25	*V72, A125*	25 (0.78)	*V72, A125*	33 (1)
			22	27.5	*V72, A125*	37 (1.2)	*V72,* A125T	13 (0.41)
KP-4	CRF01_AE	X4	0	0	–	2.1	–	2.1
			8	40	–	33 (16)	R166R/K, D279N	4.4 (2.1)
			29	40	T210I	22 (10)	G163E, R166R/K, D279N/S	4.1 (2)
89.6	B	R5X4	0	0	–	1.2	–	1.2
			8	15	–	34 (28)	–	4.4 (3.7)
			34	20	–	11 (9.2)	V180I	1.2 (1)

*Amino acid changes in each passage variant are shown. Italicized letters represent mutations relative to the consensus subtype BC or B present in the baseline isolates. Bold letters represent amino acids selected out of the quasi-species cloud. The fold increase in RAL IC_{50} values is shown in parentheses for *in vitro*-selected variants compared with those in the baseline isolates.
†The RAL variant selected after 17 passages was compared with the control selected after 20 passages.

Table 2. Comparison of amino acid length and number of PNGs between RAL-selected and control-passage KP-1 variants

	Passage no.	Genetic diversity*	Mean ENV $_{1–474}$ length (range)†	Mean V1/V2 length (range)	Mean V3 length (range)	Mean V4 length (range)	Mean PNGs (range)
Baseline	0	0.056	472 (461–480)	69 (60–74)	34 (33–34)	30 (29–31)	24 (22–28)
RAL-selected virus	2	0.038	479 (472–480)‡	74 (71–74)‡	34 (33–34)‡	31 (29–31)‡	27 (25–28) ‡
	8	0.0070	480	74	34	31	28 (26–29)
	17	0.0070	480	74	34	31	27 (26–27)§
Passage control	2	0.045	464 (461–466)‡	64 (60–74)‡	34 (33–34)‡	29 (29–31)‡	24 (22–27)‡
	8	0.0070	463 (462–463)	62	34	29	23 (22–23)
	10	0.0080	462 (459–463)	62	34	29	23 (22–23)
	20	0.010	463	62	34	29	23 (22–23)§
P value			<0.0001‡	<0.0001‡	0.91‡	0.0048‡	0.0019‡ <0.0001§

*Overall mean distance.
†Sequence from gp120 SP to the V5 region (aa 1–474).
‡, § *P* values were calculated using the homoscedastic *t*-test between the RAL-selected and the passage-control variants indicated by the same symbols above.

the whole envelope sequence [from the signal peptide (SP) to V5] were compared in the RAL-selected and passage-control viruses. The results showed that, after only two passages, the gp120, V1/V2 and V4-loop regions within RAL-selected variants were longer than those in the control variants, and the number of putative *N*-linked glycosylation sites (PNGs) was significantly higher than that in the control-passage viruses (Table 2). This phenomenon was seen consistently in two independent experiments.

We also analysed the gp120 sequences in the other four isolates. Although the number of positional differences between the RAL-selected and passage-control variants for these four isolates was lower than that in KP-1 (between three and nine, compared with >40), there was a similar pattern of separation between the Env sequences (Fig. 1). In three of the four isolates (KP-2, KP-3 and KP-4), positional differences were observed in SP, C1 and all the variable regions of gp120 (Fig. 1b–d). In strain 89.6, differences were observed in the C2, C3 and V4 regions (Fig. 1e).

These results suggested that RAL treatment of target cells causes a decrease in viral diversification within quasispecies Env regions via a route different from that in untreated target cells.

In vitro induction of RAL-selected V3-loop library virus variants

To investigate further the effects of RAL on viral Env sequences, we used the V3-loop library virus (JR-FL-V3Lib) developed by Yusa *et al.* (2005), which carries a set of random combinations from zero to ten substitutions (27 648 possibilities) in the V3 loop (residues 305, 306, 307, 308, 309, 317, 319, 322, 323 and 326; V3 loop from Cys^{296} to Cys^{331}). The variants contained in the library were polymorphic mutations derived from 31 R5 clinical isolates (Yusa *et al.*, 2005). PM1/CCR5 cells were exposed to the JR-FL-V3Lib and serially passaged in the presence of RAL. After two passages, the V3 sequence within the RAL-selected variant was completely different from that in the passage control (Fig. 1f). This suggested that, under pressure from RAL, the infectious clone harbouring different V3 region sequence from the passage control had adapted to the target cells, despite containing the same IN sequences.

Phylogenetic analysis of the Env regions after passage with or without RAL

To confirm the temporal and spatial differences observed in each of the RAL-selected and passage-control viruses, phylogenetic analyses were conducted using complete SP–V5 sequences. The neighbour-joining phylogenetic tree showed a clear and distinct branching between RAL-selected and passage-control KP-1 viruses (Fig. 2a). We also identified a similar pattern in all the other isolates tested (Fig. 2b–e).

Table 3. Comparison of amino acid length, number of potential *N*-linked glycosylation sites, V3 sequences and co-receptor usage between anti-retroviral drug-selected and control-passaged KP-1 variants

	Passage no.	Genetic diversity*	Mean ENV_{1-474} length (range)†	Mean V1/V2 length (range)	Mean V3 length (range)	Mean V4 length (range)	Mean PNGs (range)	V3 region		Geno2 pheno (%)§
								Prevalence (%)	Sequence‡	
Baseline	0	0.056	472 (461–480)	69 (60–74)	34 (33–34)	30 (29–31)	24 (22–28)	41.9	CTRPNNNTRKGIHIGPGKFYATGAIIGDIRQAHC	41.2
								22.6	.....V.....	41.2
								16.1	....-..I.....T.R..T.RD...N..K...	1.7
								13.0	....-..I.....T.R..T.KT...N.KK...	2.9
								3.2	....-..I.....	7.4
								3.2	.....D.....	55.3
Passage control	8	0.0070	463 (462–463)	62	34	29	23 (22–23)	100.0	.....V.....	41.2
RAL-selected virus	8	0.0070	480	74	34	31	28 (26–29)	100.0	.....	41.2
3TC-selected virus	6	0.020	478 (475–480)	74	34	31 (29–31)	27 (25–28)	83.3	.....	41.2
SQV-selected virus	11	0.0040	474	71	34	31	26	100.0	.....	41.2
MVC-selected virus	7	0.0080	469 (468–469)	69	33	29	24 (23–24)	100.0	....-..I....R..T.R..T.KT...N.KK...	1.7

*Overall mean distance.

†Sequence from gp120 SP to the V5 region (aa 1–474).

‡V3 sequences of each variant are shown. Dots denote sequence identity and dashes indicate a deletion mutation.

§Prediction of viral co-receptor tropism using Geno2pheno based on a selectable 'false positive rate'.

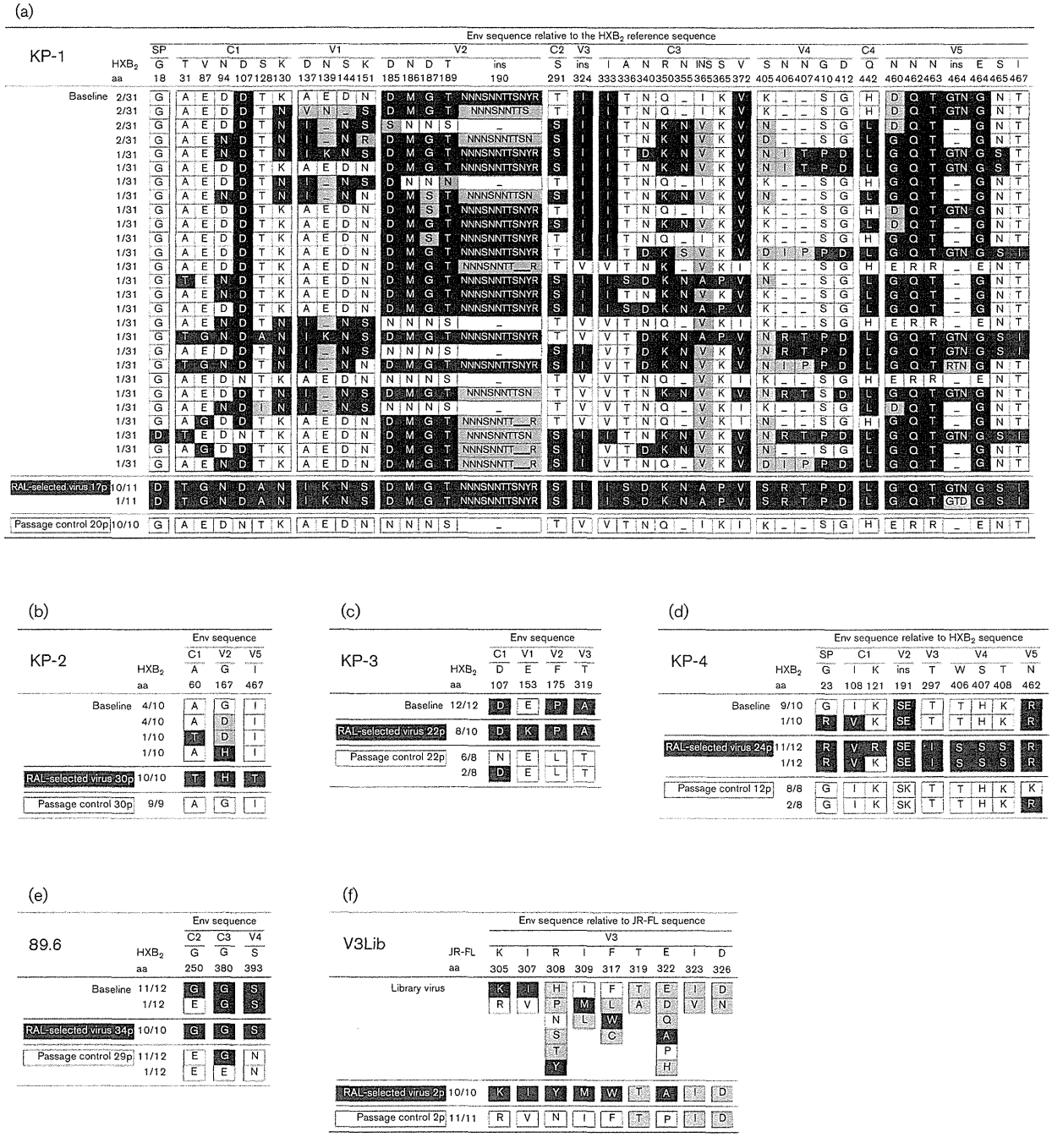

Fig. 1. Comparison of the gp120 sequences between RAL-selected and control-passaged viruses. The gp120 sequences of baseline, RAL-selected and the passage-control viruses were aligned for KP-1 (a), KP-2 (b), KP-3 (c), KP-4 (d) and strain 89.6 (e). Each amino acid in (a)–(e) is numbered relative to the HIV-1 HXB_2 reference sequence. The V3 sequences from the JR-FL-V3Lib baseline library, RAL-selected and passage-control viruses were aligned (f). Filled cells denote the most dominant amino acids observed in RAL-selected variants at the latest passage, open cells denote the most dominant amino acids observed in the passage-control variants at the latest passage and shaded cells show amino acids deleted by the end of both passages, whilst '–' indicates a deletion mutation. The number of passages is indicated, e.g. 17p for passage 17.

In vitro selection of KP-1 variants by 3TC, SQV and MVC

To determine whether other HIV drugs also changed the route of adaptation to the target cells, we attempted to select KP-1 variants using a reverse transcriptase inhibitor (3TC), a protease inhibitor (SQV) and a CCR5 inhibitor (MVC). As shown in Fig. 2(f), the pattern of clustering at distinct positions between the selected isolates and the passage-control variants was similar to that observed for the RAL-selected variants. The selected variants showed decreased diversity in the gp120 sequences; however, the length of the gp120, V1/V2 and V4 sequences increased (apart from in the MVC-selected variants). In addition, the number of PNGs within gp120 was higher than that in the control (Table 3). We also compared the V3 sequences between the passage-control and each of the drug-selected variants. The V3 sequences in all the SQV-selected variants and 83.3 % of those in the 3TC-selected variants, were comparable with those in the RAL-selected variants. This was not the case for the passage controls. Comparison of variants passaged with RAL and 3TC showed that the length of the V1/V2 and V4 regions and the number of PNGs was similar; however, these parameters were different in the SQV-selected variants (Table 3). This indicated that the time at which a drug acts (e.g. during the early or late phase of the HIV life cycle) influences the selection of Env sequences. During selection with MVC, CXCR4-tropic variants were selected from the baseline mixture after seven passages.

Taken together, these results suggested that, in treated cells, different classes of anti-HIV drugs may suppress the variability of quasi-species during *in vitro* selection via a route different from that in untreated cells.

DISCUSSION

This study evaluated the impact of anti-HIV drugs on the Env bottleneck in bulk HIV-1 primary isolates during selection *in vitro*. RAL-, 3TC- and SQV-selected variants of the unique viral isolate, KP-1, harbouring both X4 and R5 variants and with a very high level of baseline viral diversity, were used to study the final destination (genetic bottleneck) of a large variety of Env sequences. Interestingly, the phylogenetic clustering of RAL-selected KP-1 variants was completely different from that of non-drug-treated controls (Fig. 2). Our results also confirmed differences in the length of the gp120, V1/V2 and V4-loop regions and in the number of PNGs (Tables 2 and 3).

It is not clear why viruses cultured under pressure from the non-Env-directed drug RAL result in different *env* genotypes compared with those without the drug. Thus, we cloned the *IN–env* region of the proviral genome from passaged viruses and sequenced the *env* and *IN* regions on the same cloned plasmid, and compared them among the baseline and passages 1, 2, 8 and 17 of the KP-1 virus. Under low concentrations of the IN inhibitor RAL, K7 was selected for at a late passage after accumulation of the other three amino acids, K111, D278 and H216, in IN. During the sequential accumulation of these four amino acids (K111, D278, H216 and K7), the RAL-selected Env sequences at passage 17 (the Env sequences shown as filled boxes in Fig. 1) sequentially accumulated mutations in the same proviral genome (Fig. S1, available in JGV Online). However, we did not find a clone including both the RAL-selected Env at passage 17 and RAL-selected IN at passage 17 in the baseline or each passaged virus, except for in the last passage. We also examined the gp120 and IN sequences of the 3TC- and SQV-selected KP-1 variants. Compared with the RAL-selected region, the variable regions of gp120 in these selected variants were very similar to each other, except for the V1/V2 region (Fig. S2). However, the passage-control variant was very different from the drug-selected variants (Fig. 1a). Furthermore, the IN sequences were different in each passaged virus: K111/D278/H216/K7 in RAL-selected, R111/D278/Q216/R7 in 3TC-selected, K111/D278/H216/R7 in SQV-selected and R111/N278/Q216/R7 in virus without drug treatment (underlined residues indicate amino acids different from those in viruses without drug treatment). To explain these results, we believe that, under pressure from anti-HIV drugs (non-entry ARVs), the virus might show a primitive reaction to select for the Env sequence and recombine from quasi-species to gain advantage for entry and/or enhance replication in target cells. Meanwhile, IN was selected from quasi-species by a direct and/or indirect effect of RAL-induced pressure. The combination of both selective pressures may affect the selection for Env and IN during adaptation in drug-treated conditions (Figs 1a and S2). These results suggest that non-entry inhibitors, such as RAL, 3TC and SQV, might also affect cell adaptation to PM1/CCR5 cells.

Many *in vivo* studies have reported the effects of the anti-HIV drug-induced bottleneck on the *env* gene (Charpentier *et al.*, 2006; Delwart *et al.*, 1998; Ibáñez *et al.*, 2000; Kitrinos *et al.*, 2005; Nijhuis *et al.*, 1998; Nora *et al.*, 2007; Sheehy *et al.*, 1996; Zhang *et al.*, 1994). However, these studies had several limitations. Because viruses were placed under *in vivo* selective pressure using at least two anti-HIV drugs and by the host immune response, it is difficult to separate the different effects and to draw clear conclusions, particularly *in vivo*. Delwart *et al.* (1998) and Kitrinos *et al.* (2005) avoided some of these limitations by employing a heteroduplex tracking assay, although *in vivo* peculiarities still remained. Therefore, we used an *in vitro* selection system using unique bulk primary isolates established in our laboratory (Hatada *et al.*, 2010; Shibata *et al.*, 2007; Yoshimura *et al.*, 2006, 2010b) to observe the effects of the anti-retroviral drug-induced bottleneck on the *IN* and *env* genes.

This selection provides a sensitive approach for analysing virus population dynamics. The effectiveness of ARV drugs can be examined during the *in vitro* passage of a single variant or mixture of variants without being affected by many of the factors encountered *in vivo*. In addition,

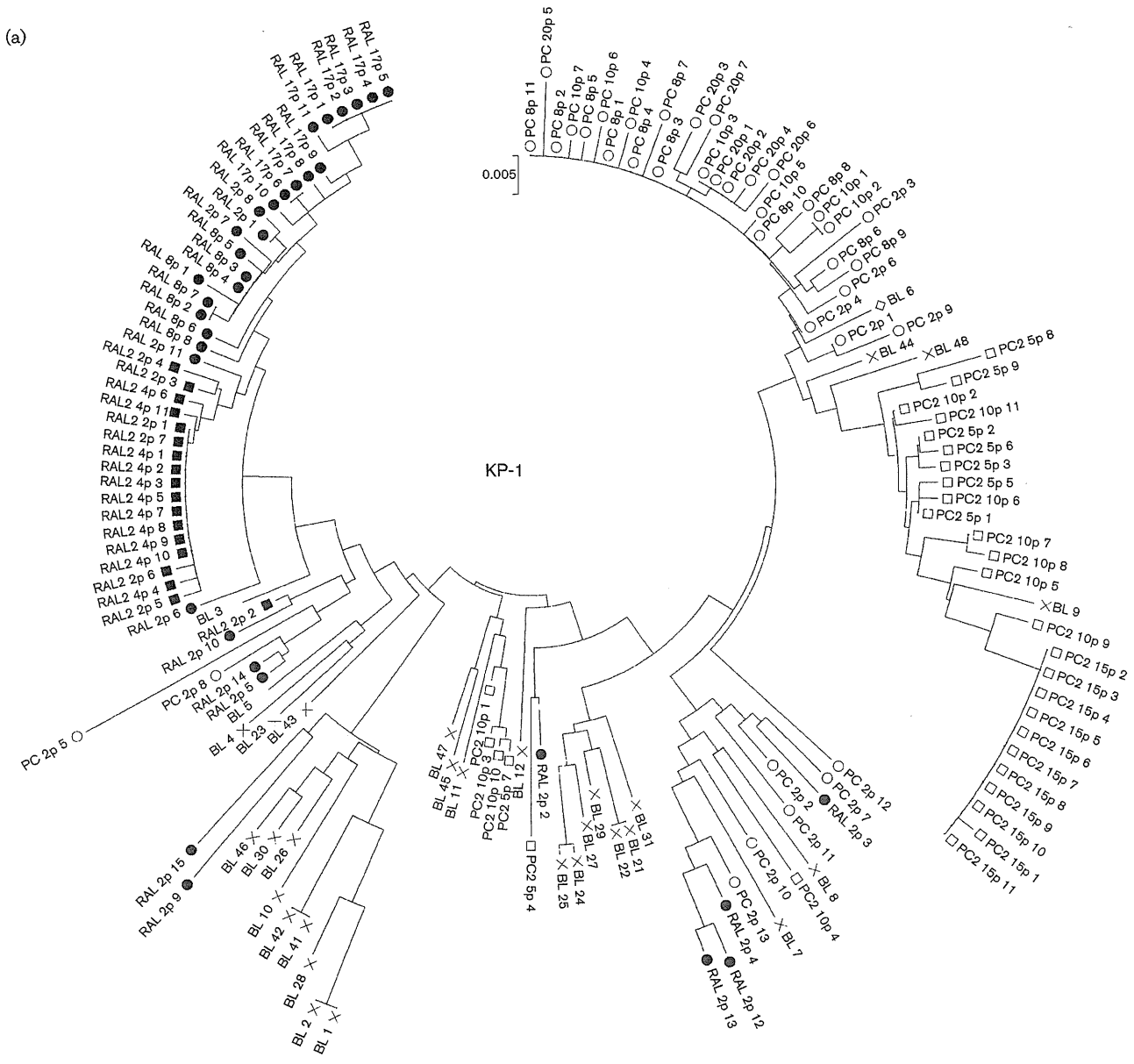

Fig. 2. Phylogenetic analyses of the Env regions from *in vitro*-passaged viruses selected with or without ARV drugs. (a–e) Phylogenetic trees were constructed using gp120 SP–V5 sequences from RAL-selected and passage-control variants of KP-1 (a), KP-2 (b), KP-3 (c), KP-4 (d) and strain 89.6 (e). An '×' represents baseline (BL) variants, and closed and open symbols represent RAL-selected (RAL) and passage-control (PC) variants, respectively. In (a), the results of the second experiment are indicated as RAL2 and PC2, respectively. (f) A phylogenetic tree was constructed using gp120 SP–V5 sequences from RAL-, 3TC-, SQV-, MVC-selected and control-passaged variants of KP-1. ○, Control variants after eight passages; ●, RAL-selected variants after eight passages; ▲, 3TC-selected variants after six passages; ◆, SQV-selected variants after 11 passages; ■, MVC-selected variants after seven passages. The trees were constructed using the neighbour-joining algorithm embedded within the MEGA software.

differences in the Env sequences between the baseline and selected variants can be compared after any number of passages. The results of the present study provide important information that will enhance our understanding of the drug-induced genetic bottleneck. This phenomenon can be examined *in vitro* using bulk primary isolates treated with or without drugs.

Recently, several new ARV drugs have been licensed for use in HIV-1-infected patients. MVC, approved in 2006, is the

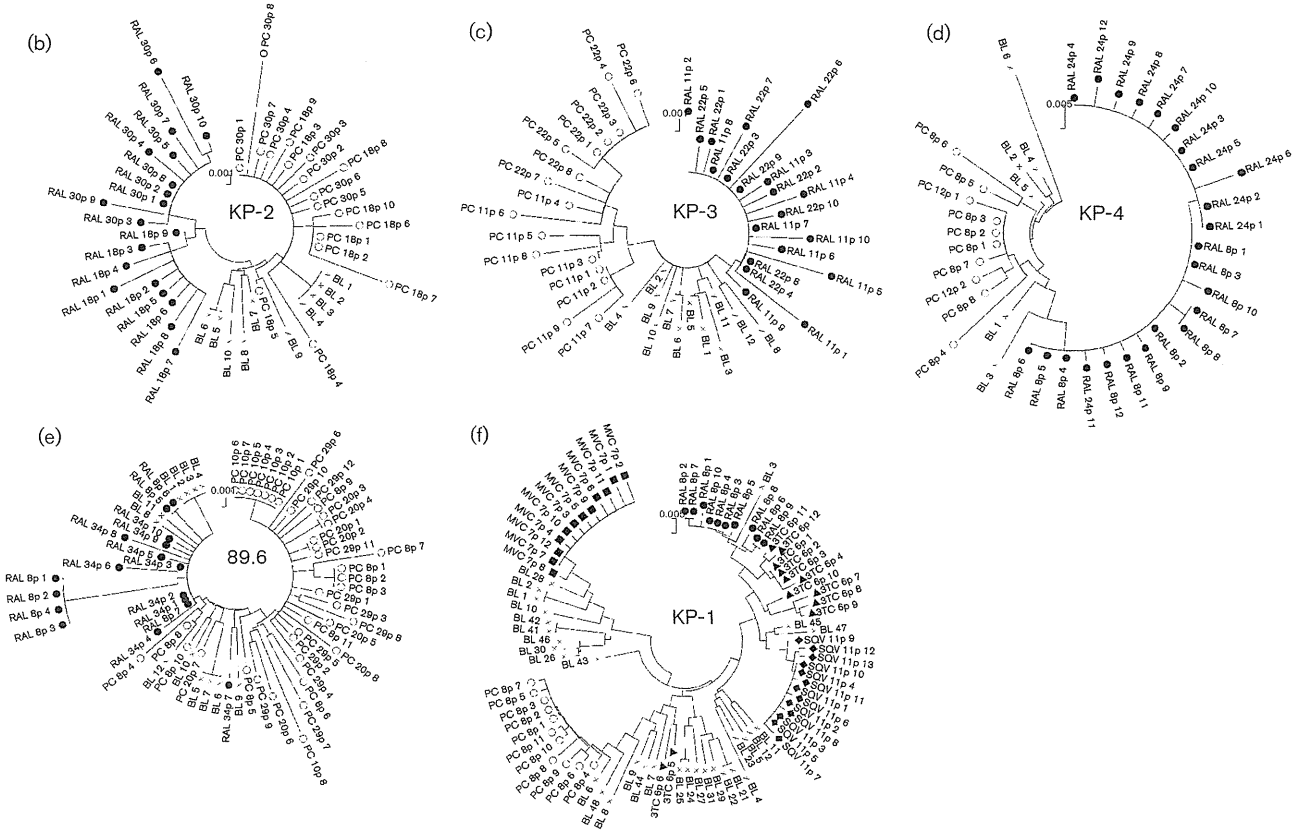

first CCR5 inhibitor (Gulick *et al.*, 2008). One important advantage associated with this drug is the absence of cross-resistance with previously available ARV compounds (Gulick *et al.*, 2008; Steigbigel *et al.*, 2008). However, as is usual with anti-HIV drugs, resistant variants with mutations in the Env, gp120 and gp41 sequences are induced both *in vivo* and *in vitro* (Anastassopoulou *et al.*, 2009; Berro *et al.*, 2009; Tilton *et al.*, 2010; Yoshimura *et al.*, 2009, 2010a). As shown in the present study, distinct Env sequences from each quasispecies might be selected by the different anti-HIV drugs (e.g. length of the V1/2 and/or V4 regions, V3 region depletion and the number of PNGs). Moreover, many of the novel anti-retroviral drugs in pre-clinical trials are viral entry inhibitors (e.g. PRO140, ibalizumab, BMS-663068 and PF-232798; Jacobson *et al.*, 2010; McNicholas *et al.*, 2010; Nettles *et al.*, 2011; Stupple *et al.*, 2011; Toma *et al.*, 2011). Therefore, it is necessary to examine whether such entry inhibitors are effective when used alongside conventional drugs.

In conclusion, we studied the genetic bottleneck in bulk primary HIV-1 isolates from untreated patients and drugs targeting the Env (and other) regions. The results showed, for the first time, the presence of drug-selected Env sequences in these isolates. Although our observations were based on a limited number of HIV-1 isolates and need to be confirmed by independent studies, we believe that they provide a new paradigm for HIV-1 evolution in the new combination ARV therapy era.

METHODS

Patients and isolates. Primary HIV-1 isolates were isolated from four drug-naïve patients in our laboratory (KP-1–4) and passaged in phytohaemagglutinin-activated PBMCs. Infected PBMCs were then co-cultured for 5 days with PM1/CCR5 cells (a kind gift from Dr Y. Maeda; Maeda *et al.*, 2008; Yusa *et al.*, 2005) and the culture supernatants were stored at −150 °C (Hatada *et al.*, 2010; Shibata *et al.*, 2007; Yoshimura *et al.*, 2006, 2010b).

After isolation of the primary viruses, we checked the sensitivity of each primary isolate to MVC. The KP-1 isolate was relatively MVC-resistant compared with KP-2 and KP-3 (54 vs 5.9 and 8.7 nM, respectively). KP-1 became MVC sensitive after eight passages in PM1/CCR5 cells [IC_{50}, 3.4 nM; Geno2pheno value (see below), 41.2 %], whilst under the pressure of MVC, KP-1 became highly resistant to MVC after eight passages (IC_{50}, >1000 nM; Geno2pheno value, 1.7 %). These results indicated that the bulk KP-1 isolate used in this study harboured primarily R5 viruses with X4- or dual-tropic viruses as a minor population.

Cells, culture conditions and reagents. PM1/CCR5 cells were maintained in RPMI 1640 (Sigma) supplemented with 10 % heat-inactivated FCS (HyClone Laboratories), 50 U penicillin ml^{-1}, 50 μg streptomycin ml^{-1} and 0.1 mg G418 (Nacalai Tesque) ml^{-1}. MVC, RAL and SQV were kindly provided by Pfizer, Merck & Co. and Roche Products, respectively. 3TC was purchased from Wako Pure Chemical Industries.

The laboratory-adapted HIV-1 strain 89.6, which was obtained through the NIH AIDS Research and Reference Reagent Program, was propagated in phytohaemagglutinin-activated PBMCs. The viral-competent library pJR-FL-V3Lib, which contains 176 bp V3–loop DNA fragments with 0–10 random combinations of amino acid substitutions, was introduced into pJR-FL, as described previously (Yusa *et al.*, 2005).

***In vitro* selection of HIV-1 variants using anti-HIV drugs.** The four primary HIV isolates (KP-1–4), strain 89.6 and JR-FL-V3Lib were treated with various concentrations of RAL and used to infect PM1/CCR5 cells to induce the production of RAL-selected HIV-1 variants, as described previously, with minor modifications (Hatada *et al.*, 2010; Shibata *et al.*, 2007; Yoshimura *et al.*, 2006, 2010b). Briefly, PM1/CCR5 cells (4×10^4 cells) were exposed to 500 $TCID_{50}$ HIV-1 isolates and cultured in the presence of RAL. Virus replication in PM1/CCR5 cells was monitored by observing the cytopathic effects. The culture supernatant was harvested on day 7 and used to infect fresh PM1/CCR5 cells for the next round of culture in the presence of increasing concentrations of RAL. When the virus began to propagate in the presence of the drug, the compound concentration was increased further. Proviral DNA was extracted from lysates of infected cells at different passages using a QIAamp DNA Blood Mini kit (Qiagen). The proviral DNAs obtained were then subjected to nucleotide sequencing. *In vitro* selection of the KP-1 isolate using SQV, 3TC and MVC was also performed using the procedure described above.

Amplification of proviral DNA and nucleotide sequencing. Proviral DNA was subjected to PCR amplification using PrimeSTAR GXL DNA polymerase and Ex-*Taq* polymerase (Takara), as described previously (Hatada *et al.*, 2010; Shibata *et al.*, 2007; Yoshimura *et al.*, 2006, 2010b). The primers used were 1B and H for the gp120 region (Hatada *et al.*, 2010; Shibata *et al.*, 2007; Yoshimura *et al.*, 2006, 2010b), IN 1F (5′-CAGACTCACAATATGCATTAGG-3′) and IN 1R (5′-CCTGTATGCAGACCCCAATATG-3′) for the *IN* region, and IN 1F and H for the *IN*–gp120 region. The first-round PCR products were used directly in a second round of PCR using primers 2B and F (Hatada *et al.*, 2010; Shibata *et al.*, 2007; Yoshimura *et al.*, 2006, 2010b) for gp120, IN 2F (5′-CTGGCATGGGTACCAGCACACAA-3′) and IN 2R (3′-CCTAGTGGGATGTGTACTTCTGAACTTA-3′) for *IN*, and IN 2F and F for *IN*–gp120. The PCR conditions used were as described above. The second-round PCR products were purified and cloned into a pGEM-T Easy Vector (Promega) or pCR-XL-TOPO Vector (Invitrogen), and the *env* and *IN* regions in both the passaged and selected viruses were sequenced using an Applied Biosystems 3500xL Genetic Analyzer and a BigDye Terminator v3.1 Cycle Sequencing kit (Applied Biosystems). Phylogenetic reconstructions were generated using the neighbour-joining method embedded in the MEGA software (http://www.megasoftware.net) (Tamura *et al.*, 2007). Overall, mean distances for viral diversity were also calculated using MEGA software. The number and location of putative PNGs were estimated using *N*-GlycoSite (http://www.hiv.lanl.gov/content/sequence/GLYCOSITE/glycosite.html) from the Los Alamos National Laboratory database.

Susceptibility assay. The sensitivity of the passaged viruses to various drugs was determined as described previously with minor modifications (Hatada *et al.*, 2010; Shibata *et al.*, 2007; Yoshimura *et al.*, 2006, 2010b). Briefly, PM1/CCR5 cells (2×10^3 cells per well) in 96-well round-bottomed plates were exposed to 100 $TCID_{50}$ of the viruses in the presence of various concentrations of drugs and incubated at 37 °C for 7 days. The IC_{50} values were then determined using a Cell Counting Kit-8 assay (Dojindo Laboratories). All assays were performed in duplicate or triplicate.

Predicting co-receptor usage by the V3 sequence. HIV-1 tropism was inferred using Geno2pheno [coreceptor] program, with a false rate positive (FPR) value of 5.0%, which is freely available (http://coreceptor.bioinf.mpi-inf.mpg.de/index.php). This genotyping tool more accurately predicts virological responses to the CCR5 antagonist MVC in ARV-naïve patients than a reference phenotypic tropism test (Sing *et al.*, 2007).

Statistical analyses. Pairwise comparisons of the different parameters between variants in the two groups was calculated using the homoscedastic *t*-test. A P value of <0.05 was considered statistically significant.

ACKNOWLEDGEMENTS

We are grateful to Dr Yosuke Maeda for providing the PM1/CCR5 cells. We also thank Syoko Yamashita, Yoko Kawanami, Noriko Shirai and Akiko Shibata for technical assistance. This study was supported in part by the Ministry of Education, Culture, Sports, Science and Technology, Japan, by a Grant-in-Aid for Young Scientists (B-22790163); grants from the Ministry of Health, Labour and Welfare; the Program of Founding Research Centers for Emerging and Re-emerging Infectious Diseases; and the Global COE program Global Education and Research Center Aiming at the Control of AIDS.

REFERENCES

Anastassopoulou, C. G., Ketas, T. J., Klasse, P. J. & Moore, J. P. (2009). Resistance to CCR5 inhibitors caused by sequence changes in the fusion peptide of HIV-1 gp41. *Proc Natl Acad Sci U S A* **106**, 5318–5323.

Berro, R., Sanders, R. W., Lu, M., Klasse, P. J. & Moore, J. P. (2009). Two HIV-1 variants resistant to small molecule CCR5 inhibitors differ in how they use CCR5 for entry. *PLoS Pathog* **5**, e1000548.

Charpentier, C., Nora, T., Tenaillon, O., Clavel, F. & Hance, A. J. (2006). Extensive recombination among human immunodeficiency virus type 1 quasispecies makes an important contribution to viral diversity in individual patients. *J Virol* **80**, 2472–2482.

Delwart, E. L., Pan, H., Neumann, A. & Markowitz, M. (1998). Rapid, transient changes at the *env* locus of plasma human immunodeficiency virus type 1 populations during the emergence of protease inhibitor resistance. *J Virol* **72**, 2416–2421.

Eigen, M. (1993). The origin of genetic information: viruses as models. *Gene* **135**, 37–47.

Gulick, R. M., Lalezari, J., Goodrich, J., Clumeck, N., DeJesus, E., Horban, A., Nadler, J., Clotet, B., Karlsson, A. & other authors (2008). Maraviroc for previously treated patients with R5 HIV-1 infection. *N Engl J Med* **359**, 1429–1441.

Hatada, M., Yoshimura, K., Harada, S., Kawanami, Y., Shibata, J. & Matsushita, S. (2010). Human immunodeficiency virus type 1 evasion of a neutralizing anti-V3 antibody involves acquisition of a potential glycosylation site in V2. *J Gen Virol* **91**, 1335–1345.

Hombrouck, A., Voet, A., Van Remoortel, B., Desadeleer, C., De Maeyer, M., Debyser, Z. & Witvrouw, M. (2008). Mutations in human immunodeficiency virus type 1 integrase confer resistance to the naphthyridine L-870,810 and cross-resistance to the clinical trial drug GS-9137. *Antimicrob Agents Chemother* **52**, 2069–2078.

Ibáñez, A., Clotet, B. & Martinez, M. A. (2000). Human immunodeficiency virus type 1 population bottleneck during indinavir therapy causes a genetic drift in the env quasispecies. *J Gen Virol* **81**, 85–95.

Jacobson, J. M., Thompson, M. A., Lalezari, J. P., Saag, M. S., Zingman, B. S., D'Ambrosio, P., Stambler, N., Rotshteyn, Y., Marozsan, A. J. & other authors (2010). Anti-HIV-1 activity of weekly or biweekly treatment with subcutaneous PRO 140, a CCR5 monoclonal antibody. *J Infect Dis* **201**, 1481–1487.

Kitrinos, K. M., Nelson, J. A., Resch, W. & Swanstrom, R. (2005). Effect of a protease inhibitor-induced genetic bottleneck on human immunodeficiency virus type 1 *env* gene populations. *J Virol* **79**, 10627–10637.

Kobayashi, M., Nakahara, K., Seki, T., Miki, S., Kawauchi, S., Suyama, A., Wakasa-Morimoto, C., Kodama, M., Endoh, T. & Oosugi, E. (2008). Selection of diverse and clinically relevant integrase inhibitor-resistant human immunodeficiency virus type 1 mutants. *Antiviral Res* **80**, 213–222.

Maeda, Y., Yusa, K. & Harada, S. (2008). Altered sensitivity of an R5X4 HIV-1 strain 89.6 to coreceptor inhibitors by a single amino acid substitution in the V3 region of gp120. *Antiviral Res* 77, 128–135.

McNicholas, P., Wei, Y., Whitcomb, J., Greaves, W., Black, T. A., Tremblay, C. L. & Strizki, J. M. (2010). Characterization of emergent HIV resistance in treatment-naive subjects enrolled in a vicriviroc phase 2 trial. *J Infect Dis* **201**, 1470–1480.

Nájera, R., Delgado, E., Pérez-Alvarez, L. & Thomson, M. M. (2002). Genetic recombination and its role in the development of the HIV-1 pandemic. *AIDS* **16** (Suppl. 4), S3–S16.

Nettles, R., Schurmann, D., Zhu, L., Stonier, M., Huang, S. P., Chien, C., Krystal, M., Wind-Rotolo, M., Bertz, R. & Grasela, D. (2011). Pharmacodynamics, safety, and pharmacokinetics of BMS-663068: a potentially first-in-class oral HIV attachment inhibitor. In *18th Conference on Retroviruses and Opportunistic Infections*, abstract 49. Boston, MA.

Nijhuis, M., Boucher, C. A., Schipper, P., Leitner, T., Schuurman, R. & Albert, J. (1998). Stochastic processes strongly influence HIV-1 evolution during suboptimal protease-inhibitor therapy. *Proc Natl Acad Sci U S A* **95**, 14441–14446.

Nora, T., Charpentier, C., Tenaillon, O., Hoede, C., Clavel, F. & Hance, A. J. (2007). Contribution of recombination to the evolution of human immunodeficiency viruses expressing resistance to antiretroviral treatment. *J Virol* **81**, 7620–7628.

Rhee, S.-Y., Liu, T. F., Kiuchi, M., Zioni, R., Gifford, R. J., Holmes, S. P. & Shafer, R. W. (2008). Natural variation of HIV-1 group M integrase: implications for a new class of antiretroviral inhibitors. *Retrovirology* 5, 74.

Sheehy, N., Desselberger, U., Whitwell, H. & Ball, J. K. (1996). Concurrent evolution of regions of the envelope and polymerase genes of human immunodeficiency virus type 1 observed during zidovudine (AZT) therapy. *J Gen Virol* 77, 1071–1081.

Shibata, J., Yoshimura, K., Honda, A., Koito, A., Murakami, T. & Matsushita, S. (2007). Impact of V2 mutations on escape from a potent neutralizing anti-V3 monoclonal antibody during in vitro selection of a primary human immunodeficiency virus type 1 isolate. *J Virol* **81**, 3757–3768.

Sing, T., Low, A. J., Beerenwinkel, N., Sander, O., Cheung, P. K., Domingues, F. S., Büch, J., Däumer, M., Kaiser, R. & other authors (2007). Predicting HIV coreceptor usage on the basis of genetic and clinical covariates. *Antivir Ther* **12**, 1097–1106.

Steigbigel, R. T., Cooper, D. A., Kumar, P. N., Eron, J. E., Schechter, M., Markowitz, M., Loutfy, M. R., Lennox, J. L., Gatell, J. M. & other authors (2008). Raltegravir with optimized background therapy for resistant HIV-1 infection. *N Engl J Med* **359**, 339–354.

Stupple, P. A., Batchelor, D. V., Corless, M., Dorr, P. K., Ellis, D., Fenwick, D. R., Galan, S. R., Jones, R. M., Mason, H. J. & other authors (2011). An imidazopiperidine series of CCR5 antagonists for the treatment of HIV: the discovery of N-(1S)-1-(3-fluorophenyl)-3-[(3-endo)-3-(5-isobutyryl-2-methyl-4,5,6,7-tetrahydro-1H-imidazo[4,5-c]pyridin-1-yl)-8-azabicyclo[3.2.1]oct-8-yl]propylacetamide (PF-232798). *J Med Chem* **54**, 67–77.

Tamura, K., Dudley, J., Nei, M. & Kumar, S. (2007). MEGA4: Molecular Evolutionary Genetics Analysis (MEGA) software version 4.0. *Mol Biol Evol* **24**, 1596–1599.

Tilton, J. C., Wilen, C. B., Didigu, C. A., Sinha, R., Harrison, J. E., Agrawal-Gamse, C., Henning, E. A., Bushman, F. D., Martin, J. N. & other authors (2010). A maraviroc-resistant HIV-1 with narrow cross-resistance to other CCR5 antagonists depends on both N-terminal and extracellular loop domains of drug-bound CCR5. *J Virol* **84**, 10863–10876.

Toma, J., Weinheimer, S. P., Stawiski, E., Whitcomb, J. M., Lewis, S. T., Petropoulos, C. J. & Huang, W. (2011). Loss of asparagine-linked glycosylation sites in variable region 5 of human immunodeficiency virus type 1 envelope is associated with resistance to CD4 antibody ibalizumab. *J Virol* **85**, 3872–3880.

Vignuzzi, M., Stone, J. K., Arnold, J. J., Cameron, C. E. & Andino, R. (2006). Quasispecies diversity determines pathogenesis through cooperative interactions in a viral population. *Nature* **439**, 344–348.

Yoshimura, K., Shibata, J., Kimura, T., Honda, A., Maeda, Y., Koito, A., Murakami, T., Mitsuya, H. & Matsushita, S. (2006). Resistance profile of a neutralizing anti-HIV monoclonal antibody, KD-247, that shows favourable synergism with anti-CCR5 inhibitors. *AIDS* **20**, 2065–2073.

Yoshimura, K., Harada, S., Hatada, M. & Matsushita, S. (2009). Mutations in V4 and C4 regions of the HIV-1 CRF08-BC envelope induced by the in vitro selection of Maraviroc Confer cross-resistance to other CCR5 inhibitors. In *16th Conference on Retroviruses and Opportunistic Infections*, p. 640. Montreal, Canada.

Yoshimura, K., Harada, S. & Matsushita, S. (2010a). Two step escape pathway of the HIV-1 subtype C primary isolate induced by the in vitro selection of Maraviroc. In *17th Conference on Retroviruses and Opportunistic Infections*, abstract 535. San Francisco, CA.

Yoshimura, K., Harada, S., Shibata, J., Hatada, M., Yamada, Y., Ochiai, C., Tamamura, H. & Matsushita, S. (2010b). Enhanced exposure of human immunodeficiency virus type 1 primary isolate neutralization epitopes through binding of CD4 mimetic compounds. *J Virol* **84**, 7558–7568.

Yusa, K., Maeda, Y., Fujioka, A., Monde, K. & Harada, S. (2005). Isolation of TAK-779-resistant HIV-1 from an R5 HIV-1 GP120 V3 loop library. *J Biol Chem* **280**, 30083–30090.

Zhang, Y. M., Dawson, S. C., Landsman, D., Lane, H. C. & Salzman, N. P. (1994). Persistence of four related human immunodeficiency virus subtypes during the course of zidovudine therapy: relationship between virion RNA and proviral DNA. *J Virol* **68**, 425–432.

Bioorganic & Medicinal Chemistry 21 (2013) 2518–2526

Contents lists available at SciVerse ScienceDirect

Bioorganic & Medicinal Chemistry

journal homepage: www.elsevier.com/locate/bmc

CD4 mimics as HIV entry inhibitors: Lead optimization studies of the aromatic substituents

Tetsuo Narumi [a], Hiroshi Arai [a], Kazuhisa Yoshimura [b,c], Shigeyoshi Harada [b,c], Yuki Hirota [a], Nami Ohashi [a], Chie Hashimoto [a], Wataru Nomura [a], Shuzo Matsushita [b], Hirokazu Tamamura [a,*]

[a] Institute of Biomaterials and Bioengineering, Tokyo Medical and Dental University, Chiyoda-ku, Tokyo 101-0062, Japan
[b] Center for AIDS Research, Kumamoto University, Kumamoto 860-0811, Japan
[c] AIDS Research Center, National Institute of Infectious Diseases, Shinjuku-ku, Tokyo 162-8640, Japan

ARTICLE INFO

Article history:
Received 22 January 2013
Revised 25 February 2013
Accepted 26 February 2013
Available online 7 March 2013

Keywords:
CD4 mimicry
Conformational change in gp120
HIV entry inhibitor
Envelope protein opener

ABSTRACT

Several CD4 mimics have been reported as HIV-1 entry inhibitors that can intervene in the interaction between a viral envelope glycoprotein gp120 and a cell surface protein CD4. Our previous SAR studies led to a finding of a highly potent analogue **3** with bulky hydrophobic groups on a piperidine moiety. In the present study, the aromatic ring of **3** was modified systematically in an attempt to improve its antiviral activity and CD4 mimicry which induces the conformational changes in gp120 that can render the envelope more sensitive to neutralizing antibodies. Biological assays of the synthetic compounds revealed that the introduction of a fluorine group as a *meta*-substituent of the aromatic ring caused an increase of anti-HIV activity and an enhancement of a CD4 mimicry, and led to a novel compound **13a** that showed twice as potent anti-HIV activity compared to **3** and a substantial increase in a CD4 mimicry even at lower concentrations.

1. Introduction

The first step of HIV entry into host cells is the interaction of a viral envelope glycoprotein gp120 with the cell surface protein CD4.[1] Such a viral attachment process is an attractive target for the development of the drugs to prevent the HIV-1 infection of its target cells.[2] Several small molecules including BMS-806,[3] IC-9564[4] and NBDs[5] have been identified that inhibit the viral attachment process by binding to gp120. Recently, we and others have been exploring the potentials of NBDs-derived CD4 mimics as a novel class of HIV entry inhibitors (Fig. 1).[6–8]

Small molecular CD4 mimics identified by an HIV syncytium formation assay showed potent cell fusion and virus cell fusion inhibitory activity against several HIV-1 laboratory and primary isolates.[5] Furthermore, the interaction of CD4 mimics with a highly conserved and functionally important pocket on gp120, known as the 'Phe43 cavity', induces conformational changes in gp120,[9] a process which occurs with unfavorable binding entropy, leading to a favorable enthalpy change similar to those caused by binding of the soluble CD4 binding to gp120. These unique properties render CD4 mimics valuable not only for the development of entry inhibitors, but which also, when combined with neutralizing antibodies function as envelope protein openers-putatively, stimulants.[10]

The structure of the complex formed by NBD-556 (**1**) bound to the gp120 core from an HIV-1 clade C strain (C1086) was recently determined by X-ray analysis (PDB: 3TGS).[11] As expected with molecular modeling by us[8a] and others,[6a] NBD-556 binds with Phe43 cavity with its *p*-chlorophenyl ring inserted into the cavity, and in addition multiple contacts were observed, with Trp112, Val255, Phe382, Ile424, Asn425, Trp427, Gly473, and Val430 of gp120 were observed (Fig. 2). However, no obvious interaction with Arg59 of CD4 was observed, although the salt bridge formation between Arg59 of CD4 and Asp368 of gp120 is a critical interaction of the viral attachment.[12] Based on this binding model, several potent compounds were recently identified.[6c,7]

Prior to those studies, we performed structure–activity relationship (SAR) studies based on the modification of the piperidine moiety of CD4 mimics to interact with Val430 and/or Asp368. These resulted in the discovery of a potent compound **3** which has bulky hydrophobic groups on its piperidine ring, and shows significant anti-HIV activity and lower cytotoxicity than other known CD4 mimics.[8c] Our study of the docking of **3** into the Phe43 cavity of gp120 suggests that the cyclohexyl group of **3** can interact hydrophobically with the isopropyl group of Val430.

We hypothesized that the optimization of the aromatic ring of **3** would lead to an increase of antiviral activity and CD4 mimicry, the latter inducing the conformational changes in gp120. Here, we de-

* Corresponding author. Tel.: +81 3 5280 8036; fax: +81 3 5280 8039.
E-mail address: tamamura.mr@tmd.ac.jp (H. Tamamura).

0968-0896/$ - see front matter © 2013 Published by Elsevier Ltd.
http://dx.doi.org/10.1016/j.bmc.2013.02.041

scribe the systematic modification of the aromatic ring of **3** for further optimization to evaluate substituent effects on anti-HIV activity, cytotoxicity and CD4 mimicry.

2. Results and discussion

The co-crystal structure of **1** with the gp120 core revealed that the aromatic group of **1** binds to gp120 by several aromatic–aromatic and hydrophobic interactions (Fig. 2). In particular, hydrophobic space surrounded by the hydrophobic amino acid residues Trp112, Val255, Phe382, and Ile424 is likely to be affected by substituents at the *meta*- and *para*-positions of the aromatic ring, and consequently we decided to investigate substituents at these positions (Fig. 3).

Initially, we selected a chlorine or a methyl group to serve as the *para*-substituent of the aromatic group because CD4 mimic compounds such as **1** (NBD-556) with a *p*-chloro substituent, and because **3** showed significant anti-HIV activity compared to other substituents. Further, CD4 mimic structures such as **2** with a *p*-methyl substituent also showed potent anti-HIV activity and exhibits lower cytotoxicity than those with the *p*-chlorophenyl derivatives.[8a] Next, we chose several halogens including F, Cl and Br, to be the *meta*-substituent on the aromatic group since previous SAR studies revealed that the introduction of an appropriate group with an electron-withdrawing ability at the *meta*-position leads to an increase of binding affinity and antiviral activity.[6a] Furthermore, to investigate whether electron withdrawal and hydrophobicity of the *meta*-position are appropriate, the CD4 mimics with a *meta*-methyl substituent, which has electron-donating properties and is similar in size to bromine, were also synthesized. Finally, two piperidine scaffolds (the 2,2,6,6-tetramethylpiperidine **A** and the dicyclohexylpiperidine **B**) were combined with these aromatics via the oxalamide linker.

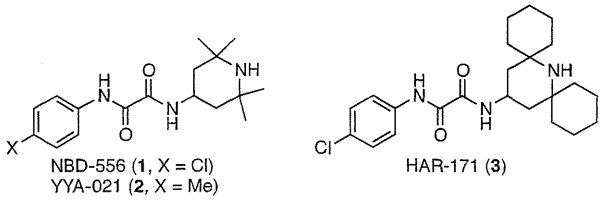

Figure 1. Structures of NBD-556 (**1**), YYA-021 (**2**) and HAR-171 (**3**).

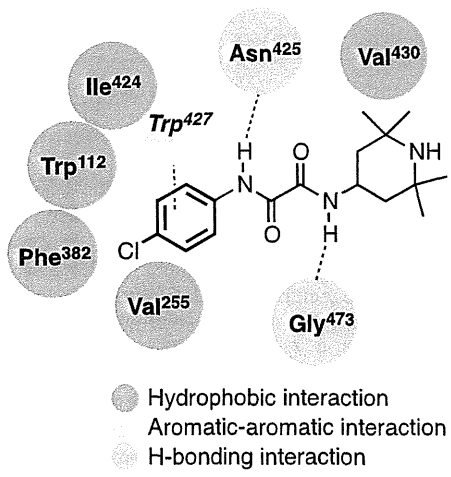

Figure 2. Major interactions between NBD-556 and Phe43 cavity of gp120.

2.1. Chemistry

The syntheses of novel compounds are depicted in Schemes 1 and 2. Starting from the appropriate aniline with *m*- and *p*-substituents, coupling with ethyl chloroglyoxylate in the presence of Et_3N gave the corresponding amidoesters **6a–c** and **7a–c**. Subsequently, microwave-assisted aminolysis[13] of **6a–c** and **7a–c** with commercially available 4-amino-2,2,6,6-tetramethylpiperidines afforded the desired compounds **8a–c** and **9a–c** (Scheme 1). A series of CD4 mimics with two cyclohexyl groups **13a–c** and **14a–c** were prepared from 2,2,6,6-tetramethylpiperidin-4-one **10** by the method previously reported,[8c] with slight modification (Scheme 2). Briefly, treatment of **10** with cyclohexanone in the presence of ammonium chloride gave a 2,6-substituted piperidin-4-one **11** via Grob fragmentation followed by intramolecular cyclization.[14] Reductive amination with *p*-methoxybenzyl amine, acidic treatment with TMSBr/TFA, and oxidative cleavage of *p*-methoxybenzyl group with cerium(IV) ammonium nitrates (CAN) furnished the corresponding 4-aminopiperidines (**12**) with higher yields and less burdensome purifications than the previous method. Finally, coupling of **12** with the corresponding esters **6a–c** and **7a–c** under microwave irradiation provided the desired compounds **13a–c** and **14a–c**.

2.2. Biological evaluation

The anti-HIV activity of the synthetic compounds was evaluated against an R5 primary isolate YTA strain. IC_{50} values were determined by the WST-8 method as the concentrations of the compounds that conferred 50% protection against HIV-1-induced cytopathogenicity in PM1/CCR5 cells. Cytotoxicity of the compounds based on the viability of mock-infected PM1/CCR5 cells was also evaluated using the WST-8 method. The assay results for compounds **8a–c** and **13a–c** with a *p*-chlorophenyl group are shown in Table 1. The parent compound **1** and compound **8a**,[6a] known as JRC-II-191, showed significant anti-HIV activities (IC_{50}

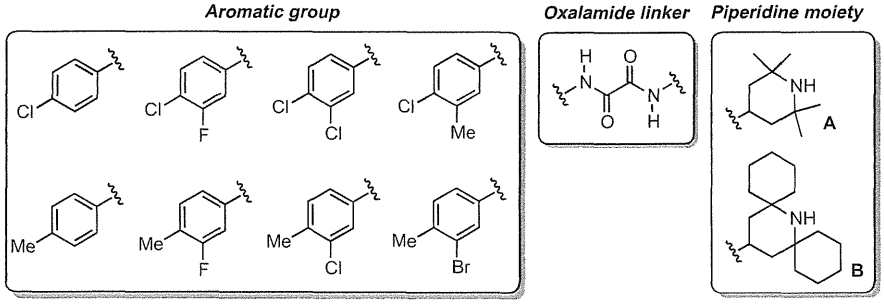

Figure 3. The structures of scaffolds in the design of novel CD4 mimics.

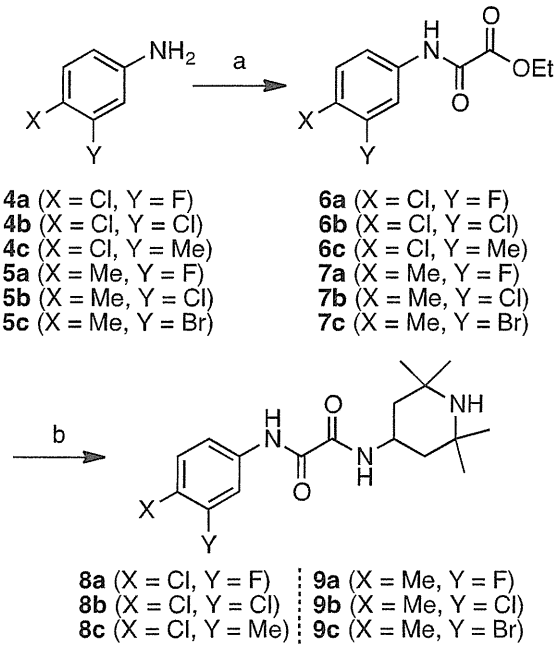

Scheme 1. Reagents and conditions: (a) ethyl chloroglyoxylate, Et_3N, THF; (b) 4-amino-2,2,6,6-tetramethylpiperidine, Et_3N, EtOH, 150 °C, microwave.

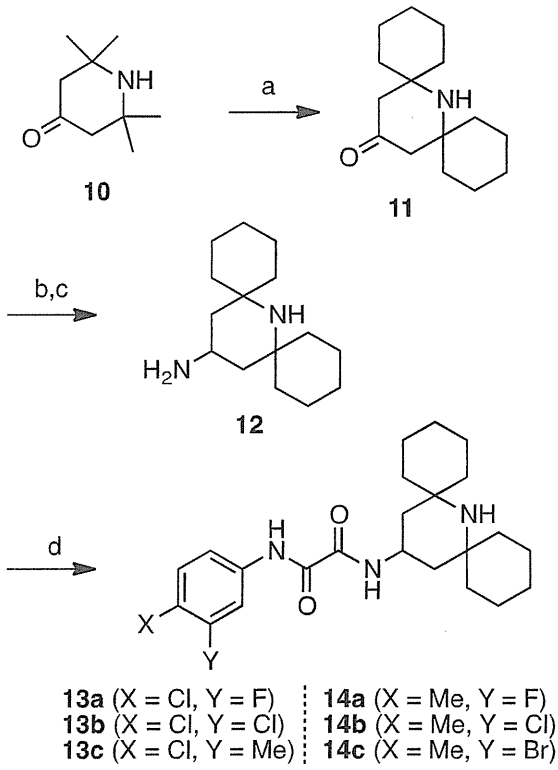

Scheme 2. Reagents and conditions: (a) cyclohexanone, NH_4Cl, DMSO, 60 °C; (b) *p*-methoxybenzylamine, $NaBH_3CN$, MeOH, then 1 M TMSBr in TFA; (c) CAN, CH_3CN/H_2O (v:v = 2:1); (d) **6** or **7**, Et_3N, EtOH, 150 °C, microwave.

of **1** = 0.61 μM and IC_{50} of **8a** = 0.32 μM). Compound **8b**[6a] having a *m,p*-dichlorophenyl group and compound **8c**[6a] (JRC-II-193) having a *p*-chloro-*m*-tolyl group showed moderate anti-HIV activity (IC_{50} of **8b** = 4.1 μM and IC_{50} of **8c** = 3.3 μM) but their potency was

Table 1
Anti-HIV activity and cytotoxicity of compounds **8a–c** and **13a–c** containing a *p*-chlorophenyl group[a]

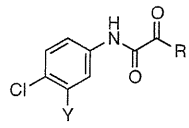

Compd	R	Y	IC_{50}[b] (μM) YTA48P	CC_{50}[c] (μM)
1	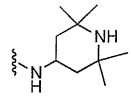	H	0.61	110
8a	**A**	F	0.32	94
8b	**A**	Cl	4.1	36
8c	**A**	Me	3.3	38
3	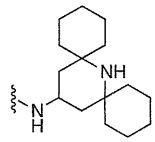	H	0.43	120
13a	**B**	F	0.23	11
13b	**B**	Cl	0.62	11
13c	**B**	Me	2.6	15

[a] All data are the mean values from three of more independent experiments.
[b] IC_{50} values of the multi-round assay are based on the inhibition of HIV-1-induced cytopathogenicity in PM1/CCR5 cells.
[c] CC_{50} values are based on the reduction of the viability of mock-infected PM1/CCR5 cells.

Table 2
Anti-HIV activity and cytotoxicity of compounds **9a–c** and **14a–c** containing a *p*-tolyl group[a]

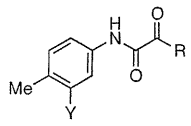

Compd	R	Y	IC_{50}[b] (μM) YTA48P	CC_{50}[c] (μM)
2	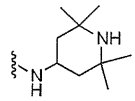	H	9.0	260
9a	**A**	F	2.8	110
9b	**A**	Cl	3.2	62
9c	**A**	Br	>10	32
14a	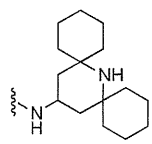	F	0.54	91
14b	**B**	Cl	6.2	11
14c	**B**	Br	3.2	11

[a] All data are the mean values from three of more independent experiments.
[b] IC_{50} values of the multi-round assay are based on the inhibition of HIV-1-induced cytopathogenicity in PM1/CCR5 cells.
[c] CC_{50} values are based on the reduction of the viability of mock-infected PM1/CCR5 cells.

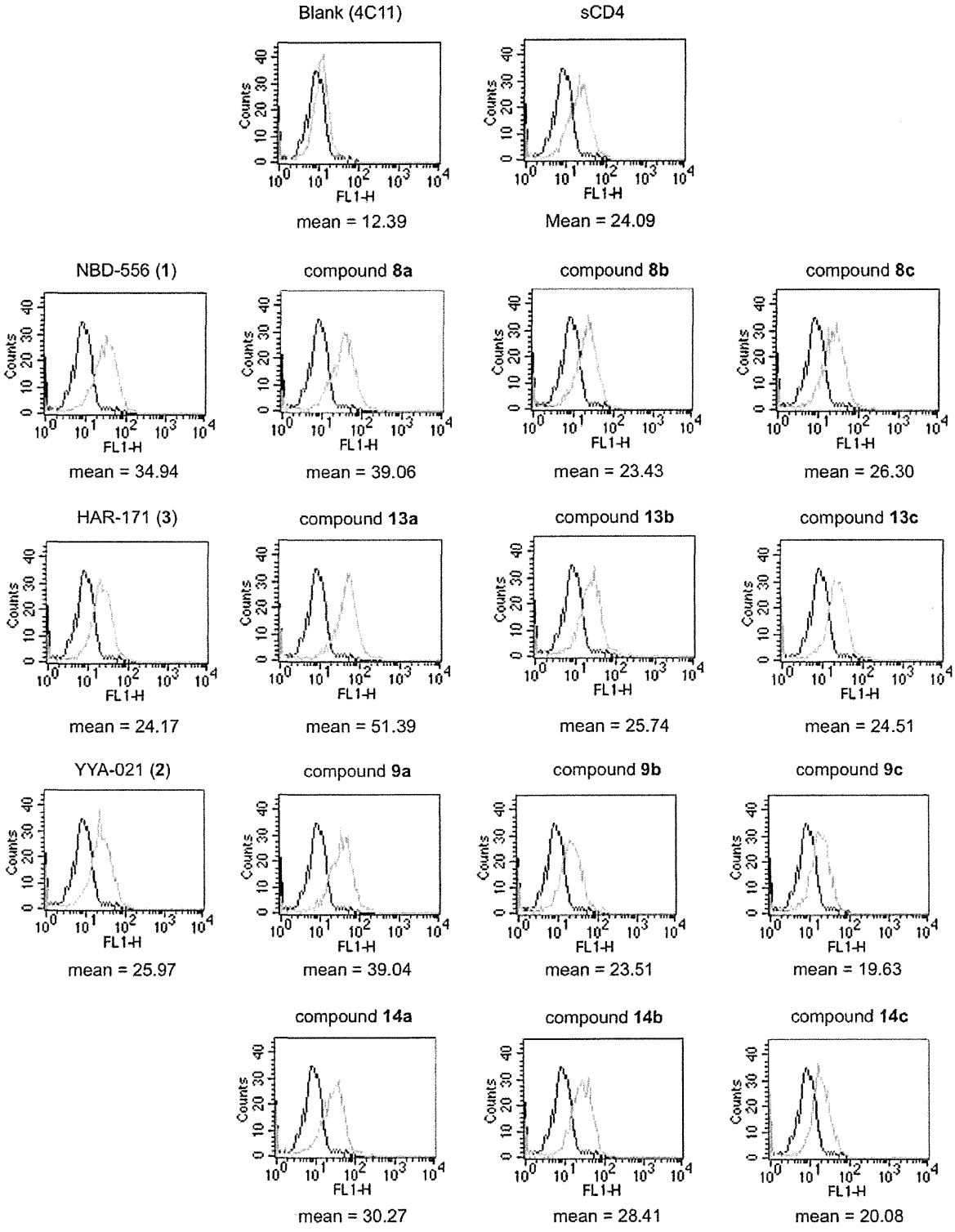

Figure 4. FACS analysis of synthetic compounds **8**, **9**, **13** and **14**.

approximately 10-fold lower than that of compound **8a**. The cytotoxicity of **8b** and **8c** is relatively stronger than that of **8a** (CC_{50} of **8b** = 36 μM and CC_{50} of **8c** = 38 μM). Compounds **13a–c** with hydrophobic cyclohexyl groups in the piperidine moiety showed more potent anti-HIV activity than the corresponding compounds **8a–c**, confirming the contribution of the bulky hydrophobic group(s) to an increase of antiviral activity. Our lead compound **3** showed significant anti-HIV activity comparable to that of compound **8a** (IC_{50} = 0.43 μM) but, consistent with previous results, exhibited lower cytotoxicity. In particular, compound **13a** with a *m*-fluoro-*p*-chlorophenyl group exhibited the highest anti-HIV activity. The IC_{50} value of **13a** was 0.23 μM, whose potency was

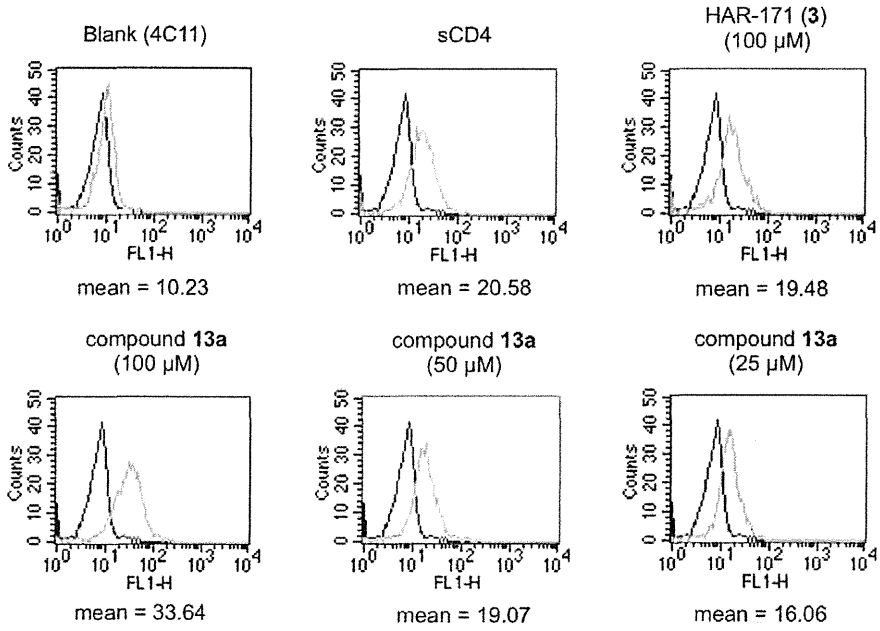

Figure 5. FACS analysis of **3** and **13a** in different concentrations.

approximately twice as high as that of compound **3**. Notably, compound **13b** with a *m,p*-dichlorophenyl group showed 7-fold more potent anti-HIV activity than the corresponding compound **8b**. Compound **13c**, which has a *p*-chloro-*m*-tolyl group, showed potent anti-HIV activity comparable to that of the corresponding compound **8c** and an increase of cytotoxicity (CC_{50} = 15 μM). We observed a tendency for compounds **13a–c** with both hydrophobic cyclohexyl groups and a *m,p*-disubstituted phenyl group to exhibit higher cytotoxicity than the corresponding tetramethyl-type compounds **8a–c**. No clear reason for an increase of cytotoxicity in the *m,p*-disubstituted phenyl group-containing compounds is apparent.

Assay results for the compounds **9a–c** and **14a–c** with a *p*-tolyl group are shown in Table 2. As expected, replacement of the *p*-chloro substituent with a *p*-methyl group resulted in somewhat reduction of anti-HIV activity. Compound **2**, YYA-021 has significant anti-HIV activity (IC_{50} = 9.0 μM) and exhibits the lowest cytotoxicity among all of the compounds tested (CC_{50} = 260 μM). These results are consistent with our previous SAR studies involving the aromatic ring. Introduction of a fluorine at the *meta*-position of the *p*-tolyl group, e.g. in compound **9a** and **14a**, improved the antiviral activity, as observed with **8a** and **13a** and a similar tendency was observed for compound **9b** with a *m*-chloro-*p*-tolyl group. In particular, compound **14a** with cyclohexyl groups and a *m*-fluoro-*p*-tolyl group showed slightly higher anti-HIV activity than the parent compound **1**. Among the compounds with *m*-bromo-*p*-tolyl groups, it was found that compound **9c**, with a 2,2,6,6-tetramethylpiperidine group, showed no anti-HIV activity at a concentration below 10 μM, whereas compound **14c** with hydrophobic cyclohexyl groups attached to the piperidine moiety, showed moderate activity (IC_{50} = 3.2 μM), indicating that the hydrophobic modification of piperidine ring can contribute to an increase in anti-HIV activity.

All the synthetic compounds were evaluated for their CD4 mimicry on the conformational changes in gp120 by fluorescence activated cell sorting (FACS) analysis, and the results are shown in Figure 4. The profile of binding of a CD4-induced (CD4i) monoclonal antibody (4C11) to the Env-expressing cell surface pretreated with the synthetic compounds was assessed in terms of the mean fluorescence intensity (MFI). The increase in binding affinity for 4C11 (by the pretreatment with synthetic compounds) suggests that those compounds can reflect the CD4 mimicry as a consequence of the conformational changes in gp120. Our previous studies disclosed that the profiles of the binding to the cell surface pretreated with **1**, **2**, or **3** were similar to those observed in pretreatment with soluble CD4, indicating that these compounds offer a significant enhancement of binding affinity for 4C11.[8] As shown in Figure 4, similar results were obtained with those compounds in this FACS analysis (MFI of **1**, **2**, and **3** = 34.94, 25.97, and 24.17, respectively). A notable increase in binding affinity for 4C11 was observed in essentially all the synthetic compounds. The compounds **8a**, **9a**, **13a** and **14a** with a *meta*-fluorine in the aromatic ring, showed significant anti-HIV activity, and produced a substantial increase in binding affinity for 4C11. These results suggested that the introduction of a fluorine group at the meta position of the aromatic ring is significant not only for the increase of anti-HIV activity, but also for the enhancement of a CD4 mimicry. In particular, a remarkable improvement in binding affinity for 4C11 was observed with **13a** (MFI = 51.39) which has twofold more potent anti-HIV activity than the lead compound **3** (HAR-171), and is the most active compound in terms of both anti-HIV activity and the CD4 mimicry resulting from the conformational change in gp120. The profiles of pretreatment of the cell surface with compounds **8b** and **13b** having a *m,p*-dichlorophenyl group, compounds **8c** and **13c** having a *p*-chloro-*m*-tolyl group, and compounds **9b** and **14b** with a *m*-chloro-*p*-tolyl group were similar to results obtained for **3**, suggesting that these compounds produced slightly lower enhancement compared to those of compounds **8a**, **9a**, **13a** and **14a** but significant levels of binding affinity for 4C11. On the other hand, pretreatment with compounds **9c**, which failed to show significant anti-HIV activity and **14c**, which had moderate anti-HIV activity resulted in a slight decrease of binding affinity for 4C11, suggesting that the introduction of a Br group at the *meta*-position of *p*-tolyl group is not advantageous to a CD4 mimicry, possibly due to the steric hindrance caused by the two bulky substituents. These results are consistent with previous observations that a limited size and electron-withdrawing ability of the aromatic substituents are required for potent anti-HIV activity and CD4 mimicry.[8a]

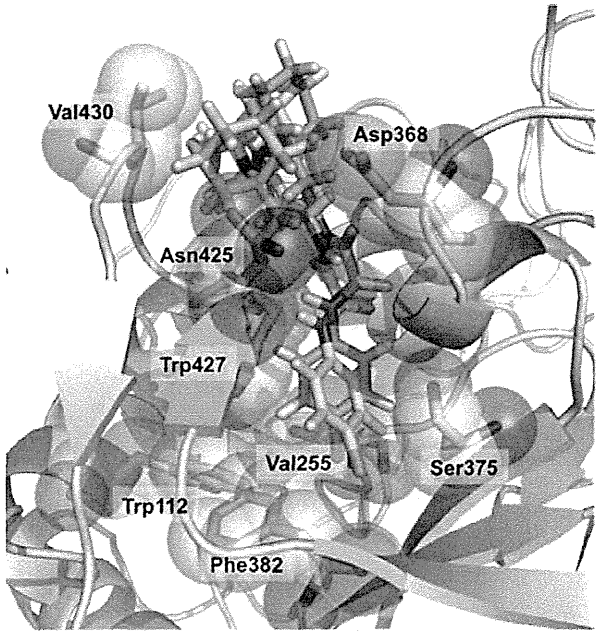

Figure 6. The modeled structure of **13a** (yellow carbon atoms) in the complex with the Phe43 cavity in gp120 (3TGS) overlaid with the modeled structure of **3** (green carbon atoms).

Since **13a** showed higher CD4 mimicry than the other compounds tested, the effect of the solution concentration of **13a** on the binding affinity for 4C11 was investigated. As shown in Figure 5, pretreatment of the cell surface with a 100 μM solution of **13a** produced a higher increase in the binding affinity for 4C11 than pretreatment with the same concentration of compound **3**. Interestingly, the profile pretreated with a 50 μM solution of **13a** was similar to that with a 100 μM of compound **3**, and even with a 25 μM solution of **13a** a potent enhancement of the binding affinity for 4C11 was observed: MFI of **13a** at concentrations of 50 μM and 25 μM = 19.07 and 16.06, respectively. This observation suggests that **13a** could serve as a novel lead compound for the development of envelope protein openers for the use combined with neutralizing antibodies because of its effectiveness at low concentrations.

The substantial increase in the CD4 mimicry of **13a** even at a low concentration is not easily explained because HAR-171 (**3**) and **13a** would be expected to form the similar binding modes with gp120. A probable contribution of **13a** is suggested by modeling studies docked into the Phe43 cavity in gp120 (3TGS) in which the depth and direction of the aromatic ring of **13a** is slightly different from those in compound **3** (Fig. 6), leading to the possible formation of appropriate interactions with the hydrophobic amino acid residues such as Val255 and Phe382, and therefore explaining the increased potency observed in the anti-HIV activity and CD4 mimicry of **13a**.

3. Conclusion

CD4 mimics are attractive agents not only for the development of a novel class of HIV entry inhibitors but also as possible cooperating agents for the neutralizing antibodies—that is, envelope protein openers. In the present study, a structure–activity relationship study of a series of CD4 mimic compounds was performed with a view to improving the biological activity of HAR-171 (**3**), which was identified in our previous studies as a promising lead compound with anti-HIV activity, cytotoxicity and CD4 mimicry resulting from the conformational change in gp120. Systematic modification of the *meta*- and *para*-substituents of the aromatic ring of **3** led to some potent compounds. In particular, **13a**, which has a bulky hydrophobic group on its piperidine ring and a *m*-fluoro-*p*-chlorophenyl group, demonstrated twofold more potent anti-HIV activity and much higher CD4 mimicry than **2** following the conformational changes in gp120, although the cytotoxicity of **13a** is relatively high. Further structural modification studies of the aromatic ring and the oxalamide linker to improve pharmaceutical profiles will be the subject of future reports.

4. Experimentals

^{1}H NMR and ^{13}C NMR spectra were recorded using a Bruker Avance III spectrometer. Chemical shifts are reported in δ (ppm) relative to Me_4Si (in $CDCl_3$) as internal standard. Low- and high-resolution mass spectra were recorded on a Bruker Daltonics microTOF focus in the positive and negative detection mode. For flash chromatography, silica gel 60 N (Kanto Chemical Co., Inc.) was employed. Microwave reactions were performed in Biotage Microwave Reaction Kit (sealed vials) in an Initiator™ (Biotage). The wattage was automatically adjusted to maintain the desired temperature for the desired period of time.

4.1. Chemistry

4.1.1. Ethyl 2-((4-chloro-3-fluorophenyl)amino)-2-oxoacetate (6a)

To a stirred solution of 3-fluoroaniline (1.11 g, 10.0 mmol) in $CHCl_3$ (30.0 mL) was added dropwise *N*-chlorosuccinimide (NCS) in $CHCl_3$ (20.0 mL) at 0 °C. The mixture was stirred at 0 °C for 42 h. After the reaction mixture was concentrated under reduced pressure, the residue was dissolved in Et_2O. The mixture was washed with water, and dried over $MgSO_4$. Concentration under reduced pressure followed by flash chromatography over silica gel with EtOAc/*n*-hexane gave 4-chloro-3-fluoroaniline (259.4 g, 18% yield) as crystalline solids. To a stirred solution of the above aniline (259.4 mg, 1.78 mmol) in THF (8.9 mL) were added at 0 °C ethyl chloroglyoxylate (237.3 μL, 2.14 mmol) and Et_3N (296.6 μL, 2.14 mmol). The mixture was stirred at room temperature for 12 h. After the precipitate was filtrated off, the filtrate solution was concentrated under reduced pressure. The residue was dissolved in EtOAc, and washed with 1.0 M HCl, saturated $NaHCO_3$ and brine, then dried over $MgSO_4$. Concentration under reduced pressure to provide the title compound **6a** (435.2 mg, 99% yield) as brown crystals, which was used without further purification.

^{1}H NMR (500 MHz, $CDCl_3$) δ 1.44 (t, J = 7.50 Hz, 3H), 4.43 (q, J = 7.50 Hz, 2H), 7.24–7.25 (m, 1H), 7.35–7.40 (m, 1H), 7.70–7.75 (m, 1H), 8.93 (br, 1H); ^{13}C NMR (125 MHz, $CDCl_3$) δ 13.0, 64.1, 108.5 (d, J = 26.3 Hz), 115.9 (d, J = 3.75 Hz), 117.3 (d, J = 18.8 Hz), 130.9 (d, J = 10.0 Hz), 135.9, 153.9, 158.1 (d, J = 246.3 Hz), 160.5; HRMS (ESI), *m/z* calcd for $C_{10}H_{10}ClFNO_3$ (MH^-) 244.0182, found 244.0183.

4.1.2. Ethyl 2-((3,4-dichlorophenyl)amino)-2-oxoacetate (6b)

To a stirred solution of 3,4-dichloroaniline **4b** (1.94 g, 12.0 mmol) in THF (20.0 mL) were added ethyl chloroglyoxylate (1.11 mL, 10.0 mmol) and Et_3N (15.2 mL, 11.0 mmol) at 0 °C. The mixture was stirred at room temperature for 6 h. After the precipitate was filtrated off, the filtrate solution was concentrated under reduced pressure. The residue was dissolved in EtOAc, and washed with 1.0 M HCl, saturated $NaHCO_3$ and brine, then dried over $MgSO_4$. Concentration under reduced pressure to provide the title compound **6b** (1.58 g, 95% yield) as white powder, which was used without further purification.

^{1}H NMR (500 MHz, $CDCl_3$) δ 1.44 (t, J = 7.00 Hz, 3H), 4.43 (q, J = 7.00 Hz, 2H), 7.44 (d, J = 8.50 Hz, 1H), 7.49–7.51 (m, 1H), 7.87, 2.35 (d, J = 2.50 Hz, 1H); ^{13}C NMR (125 MHz, $CDCl_3$) δ 14.0, 64.0, 119.0, 121.5, 129.0, 130.8, 133.2, 135.7, 153.9, 160.5; HRMS (ESI), m/z calcd for $C_{10}H_{10}Cl_2NO_3$ (MH^+) 262.0038, found 262.0031.

4.1.3. Ethyl 2-((4-chloro-3-methylphenyl)amino)-2-oxoacetate (6c)

By use of a procedure similar to that described for the preparation of compound **6b**, the aniline **4c** (3.34 g, 24.0 mmol) was converted into the title compound **6c** (4.63 g, 96% yield) as white powder.

^{1}H NMR (500 MHz, $CDCl_3$) δ 1.43 (t, J = 7.00 Hz, 3H), 2.38 (s, 3H), 4.42 (q, J = 7.00 Hz, 2H), 7.33 (d, J = 8.50 Hz, 1H), 7.43–7.46 (m, 1H), 7.51–7.54 (m, 1H), 8.82 (s, 1H); ^{13}C NMR (125 MHz, $CDCl_3$) δ 14.0, 20.2, 63.8, 118.5, 122.0, 129.7, 130.9, 134.8, 137.1, 153.8, 160.9; HRMS (ESI), m/z calcd for $C_{11}H_{13}ClNO_3$ (MH^+) 242.0578, found 242.0568.

4.1.4. Ethyl 2-((3-fluoro-4-methylphenyl)amino)-2-oxoacetate (7a)

By use of a procedure similar to that described for the preparation of compound **6b**, the aniline **5a** (3.00 g, 24.0 mmol) was converted into the title compound **7a** (4.24 g, 94% yield) as white powder.

^{1}H NMR (500 MHz, $CDCl_3$) δ 1.43 (t, J = 7.20 Hz, 3H), 2.25 (s, 3H), 4.42 (q, J = 6.80 Hz, 2H), 7.12–7.21 (m, 2H), 7.48–7.56 (m, 1H), 8.83 (s, 1H); ^{13}C NMR (125 MHz, $CDCl_3$) δ 14.2 (2C), 63.8, 107.1 (d, J = 27.5 Hz), 115.0 (d, J = 10.0 Hz), 122.3 (d, J = 17.5 Hz), 131.6 (d, J = 6.25 Hz), 135.3 (d, J = 13.8 Hz), 153.8, 160.8, 161.1 (d, J = 243.8 Hz); HRMS (ESI), m/z calcd for $C_{11}H_{13}FNO_3$ (MH^+) 226.0879, found 226.0878.

4.1.5. Ethyl 2-((3-chloro-4-methylphenyl)amino)-2-oxoacetate (7b)

By use of a procedure similar to that described for the preparation of compound **6b**, the aniline **5b** (3.40 g, 24.0 mmol) was converted into the title compound **7b** (5.19 g, 94% yield) as white powder.

^{1}H NMR (500 MHz, $CDCl_3$) δ 1.43 (t, J = 7.00 Hz, 3H), 2.35 (s, 3H), 4.42 (q, J = 7.00 Hz, 2H), 7.22 (d, J = 8.50 Hz, 1H), 7.41–7.43 (m, 1H), 7.71 (d, J = 2.00 Hz, 1H), 8.83 (s, 1H); ^{13}C NMR (125 MHz, $CDCl_3$) δ 14.0, 20.0, 63.8, 118.0, 120.3, 131.2, 133.3, 134.7, 135.0, 153.8, 160.8; HRMS (ESI), m/z calcd for $C_{11}H_{13}ClNO_3$ (MH^+) 242.0584, found 242.0573.

4.1.6. Ethyl 2-((3-bromo-4-methylphenyl)amino)-2-oxoacetate (7c)

By use of a procedure similar to that described for the preparation of compound **6b**, the aniline **5c** (4.47 g, 27.0 mmol) was converted into the title compound **7c** (6.24 g, 96% yield) as white powder.

^{1}H NMR (500 MHz, $CDCl_3$) δ 1.43 (t, J = 7.00 Hz, 3H), 2.38 (s, 3H), 4.42 (q, J = 7.00 Hz, 2H), 7.23 (t, J = 8.50 Hz, 1H), 7.48–7.53 (m, 1H), 7.83–7.90 (m, 1H), 8.80 (s, 1H); ^{13}C NMR (125 MHz, $CDCl_3$) δ 14.0, 22.4, 63.9, 118.7, 123.4, 125.0, 131.0, 135.0, 135.2, 153.7, 160.8; HRMS (ESI), m/z calcd for $C_{11}H_{13}BrNO_3$ (MH^+) 286.0079, found 286.0068.

4.1.7. N^1-(4-Chloro-3-fluorophenyl)-N^2-(2,2,6,6-tetramethylpiperidin-4-yl)oxalamide (8a)

To a solution of compound **6a** (70.0 mg, 0.286) in EtOH (2.9 mL) were added Et_3N (0.200 mL, 1.45 mmol) and 2,2,6,6-tetramethylpiperidin-4-amine (0.150 mL, 0.870 mmol). The reaction mixture was stirred for 3 h at 150 °C under microwave irradiation. After being concentrated in vacuo, the residue was extracted with $CHCl_3$, and washed with saturated $NaHCO_3$ and brine, then dried over $MgSO_4$. Concentration under reduced pressure to provide the title compound **8a** (34.6 mg, 34% yield) as white powder.

^{1}H NMR (500 MHz, $CDCl_3$) δ 0.99–1.50 (m, 15H), 1.92 (dd, J = 3.50, 9.00 Hz, 2H), 4.20–4.32 (m, 1H), 7.21–7.25 (m, 1H), 7.34–7.41 (m, 1H), 7.69–7.73 (m 1H), 9.31 (br, 1H); ^{13}C NMR (125 MHz, $CDCl_3$) δ 28.4, 34.8, 43.8, 44.5, 51.0, 108.3 (d, J = 26.3 Hz), 115.8 (d, J = 3.75 Hz), 117.1 (d, J = 17.5 Hz), 130.8, 136.2 (d, J = 8.75 Hz), 157.6, 158.1 (d, J = 247.5 Hz), 158.4; HRMS (ESI), m/z calcd for $C_{17}H_{24}ClFN_3O_2$ (MH^+) 356.1536, found 356.1548.

4.1.8. N^1-(3,4-Dichlorophenyl)-N^2-(2,2,6,6-tetramethylpiperidin-4-yl)oxalamide (8b)

By use of a procedure similar to that described for the preparation of compound **8a**, the compound **6b** (261.0 mg, 1.00 mmol) was converted into the title compound **8b** (520.0 mg, 70% yield) as white powder.

^{1}H NMR (500 MHz, $CDCl_3$) δ 1.07 (t, J = 12.0 Hz, 2H), 1.16 (s, 6H), 1.28 (s, 6H), 1.90–1.93 (m, 2H), 4.20–4.32 (m, 1H), 7.26 (m, 1H), 7.40–7.48 (m, 2H), 7.88 (s, 1H), 9.33 (s, 1H); ^{13}C NMR (125 MHz, $CDCl_3$) δ 28.5 (2C), 34.9 (2C), 43.8, 44.6 (2C), 50.9 (2C), 119.0, 121.4, 128.7, 130.8, 133.1, 135.8, 157.7, 158.5; HRMS (ESI), m/z calcd for $C_{17}H_{22}Cl_2N_3O_2$ (MH^-) 370.1095, found 370.1105.

4.1.9. N^1-(4-Chloro-3-methylphenyl)-N^2-(2,2,6,6-tetramethylpiperidin-4-yl)oxalamide (8c)

By use of a procedure similar to that described for the preparation of compound **8a**, the compound **6c** (482.0 mg, 2.00 mmol) was converted into the title compound **8c** (364.0 mg, 49% yield) as white powder.

^{1}H NMR (500 MHz, $CDCl_3$) δ 1.07 (t, J = 12.0 Hz, 2H), 1.15 (s, 6H), 1.28 (s, 6H), 1.86–1.94 (m, 2H), 4.15–4.31 (m, 1H), 7.21–7.24 (m, 1H), 7.32–7.38 (m, 2H), 7.74 (s, 1H), 9.24 (s, 1H); ^{13}C NMR (125 MHz, $CDCl_3$) δ 19.6, 28.5 (2C), 34.9 (2C), 43.7, 44.7 (2C), 50.9 (2C), 117.9, 120.2, 131.2, 133.1, 134.7, 135.1, 157.5, 158.8; HRMS (ESI), m/z calcd for $C_{18}H_{25}ClN_3O_2$ (MH^-) 350.1641, found 350.1656.

4.1.10. N^1-(3-Fluoro-4-methylphenyl)-N^2-(2,2,6,6-tetramethylpiperidin-4-yl)oxalamide (9a)

By use of a procedure similar to that described for the preparation of compound **8a**, the compound **7a** (225.0 mg, 1.00 mmol) was converted into the title compound **9a** (161.0 mg, 48% yield) as white powder.

^{1}H NMR (500 MHz, $CDCl_3$) δ 1.07 (t, J = 12.5 Hz, 2H), 1.15 (s, 6H), 1.28 (s, 6H), 1.92 (dd, J = 12.5, 3.50 Hz, 2H), 2.26 (s, 3H), 4.12–4.32 (m, 1H), 7.12–7.20 (m, 2H), 7.30–7.37 (m, 1H), 7.48–7.54 (m, 1H), 9.27 (s, 1H); ^{13}C NMR (125 MHz, $CDCl_3$) δ 14.2, 28.5 (2C), 34.9 (2C), 43.7, 44.7 (2C), 50.9 (2C), 107.1 (d, J = 26.3 Hz), 115.0, 121.8 (d, J = 17.5 Hz) 131.6, 135.4, (d, J = 15.0 Hz), 157.5, 158.8, 161.1 (d, J = 242.5 Hz); HRMS (ESI), m/z calcd for $C_{18}H_{25}FN_3O_2$ (MH^-) 334.1936, found 334.1942.

4.1.11. N^1-(3-Chloro-4-methylphenyl)-N^2-(2,2,6,6-tetramethylpiperidin-4-yl)oxalamide (9b)

By use of a procedure similar to that described for the preparation of compound **8a**, the compound **7b** (482.0 mg, 1.00 mmol) was converted into the title compound **9b** (448.0 mg, 48% yield) as white powder.

^{1}H NMR (500 MHz, $CDCl_3$) δ 1.09 (t, J = 12.5 Hz, 3H), 1.18 (s, 6H), 1.30 (s, 6H), 1.93–1.95 (m, 2H), 2.41 (s, 3H), 4.20–4.34 (m, 1H), 7.30–7.37 (m, 2H), 7.44–7.46 (m, 1H), 7.53 (d, J = 2.50 Hz, 1H), 9.25 (s, 1H); ^{13}C NMR (125 MHz, $CDCl_3$) δ 20.3, 28.5 (2C), 34.9 (2C), 43.7, 44.7 (2C), 50.9 (2C), 118.5, 122.0, 130.0, 130.7, 134.8, 137.1, 157.5, 158.8; HRMS (ESI), m/z calcd for $C_{18}H_{25}ClN_3O_2$ (MH^-) 350.1641, found 350.1636.

4.1.12. N^1-(3-Bromo-4-methylphenyl)-N^2-(2,2,6,6-tetramethylpiperidin-4-yl)oxalamide (9c)

By use of a procedure similar to that described for the preparation of compound **8a**, the compound **7c** (285.0 mg, 1.00 mmol) was converted into the title compound **9c** (157.0 mg, 40% yield) as white powder.

^{1}H NMR (500 MHz, $CDCl_3$) δ 1.07 (t, J = 12.5 Hz, 3H), 1.15 (s, 6H), 1.28 (s, 6H), 1.91 (dd, J = 8.00, 4.00 Hz, 2H), 2.38 (s, 3H), 3.70–3.75 (m, 1H), 7.22 (d, J = 8.50 Hz, 1H), 7.30–7.37 (m, 1H), 7.43–7.45 (m, 1H), 7.90 (d, J = 2.50 Hz, 1H), 9.25 (s, 1H); ^{13}C NMR (125 MHz, $CDCl_3$) δ 22.4, 28.5 (2C), 34.9 (2C), 43.7, 44.7 (2C), 50.9 (2C), 118.6, 123.4, 125.0, 131.0, 134.9 (2C), 157.5, 158.8; HRMS (ESI), m/z calcd for $C_{18}H_{25}BrN_3O_2$ (MH^-) 394.1136, found 394.1158.

4.1.13. Amine (12)

The compound **11** was prepared according to the reported procedure.[14] To a stirred solution of piridone **11** (247.8 mg, 1.05 mmol) in MeOH (2.10 mL) was added *p*-methoxybenzylamine (0.41 mL, 3.15 mmol). After being stirred at room temperature for 23 h, sodium cyanoborohydride was added and stirred at room temperature for 48 h. The reaction mixture was poured into saturated $NaHCO_3$ and extracted with EtOAc, then dried over $MgSO_4$. After concentration under reduced pressure, the residue was treated with 1 M TMS in THF (4.8 mL). The mixture was stirred at 0 °C for 14 h. Concentration under reduced pressure followed by short chromatography with $CHCl_3$/MeOH gave the PMB-protected amine. To a solution of the above amine (584.0 mg, 1.64 mmol) in CH_3CN/H_2O (13.1 mL, v:v = 2:1) was added CAN (2.74 g, 8.2 mmol). The mixture was stirred at room temperature for 14 h. The reaction mixture was diluted with 0.5 M HCl and washed with CH_2Cl_2. The water layer was alkalized and extracted with EtOAc, then dried over Na_2SO_4. Concentration under reduced pressure followed by flash chromatography over silica gel with EtOAc–EtOH (4:1) to gave the title compound **12** (175.5 mg, 71% yield) as a yellow oil.

^{1}H NMR (500 MHz, $CDCl_3$) δ 1.15–1.85 (m, 24H), 2.95–3.05 (m, 1H); ^{13}C NMR (125 MHz, $CDCl_3$) δ 22.2 (2C), 22.8 (2C), 26.2 (2C), 37.3 (2C), 42.3 (2C), 43.6 (2C), 47.0, 53.2 (2C); HRMS (ESI), m/z calcd for $C_{15}H_{29}N_2$ (MH^+) 237.2325, found 237.2321.

4.1.14. N^1-((4-Chloro-3-fluorophenyl)-N^2-(2,6-dicyclohexylpiperidin-4-yl)oxalamide (13a)

By use of a procedure similar to that described for the preparation of compound **8a**, the compound **6a** (36.8 mg, 0.150 mmol) was converted into the title compound **13a** (7.6 mg, 12% yield) as yellow powder.

^{1}H NMR (400 MHz, $CDCl_3$) δ 0.71–2.28 (m, 24H), 2.03–2.20 (m, 2H), 4.02–4.16 (m, 1H), 7.13–7.18 (m, 1H), 7.27–7.33 (m, 1H), 7.62–7.66 (m, 1H), 9.25 (br, 1H); ^{13}C NMR (125 MHz, $CDCl_3$) δ 14.1, 22.0 (2C), 22.6 (2C), 25.8 (2C), 29.3, 29.7 (2C), 31.9, 70.5, 108.3 (d, J = 26.3 Hz), 115.8, 117.1 (d, J = 18.8 Hz), 130.8, 136.2 (d, J = 10.0 Hz), 157.6, 158.1 (d, J = 247.5 Hz), 158.6; HRMS (ESI), m/z calcd for $C_{23}H_{32}ClFN_3O_2$ (MH^+) 436.2162, found 436.2156.

4.1.15. N^1-(4-Chlorophenyl)-N^2-(2,6-dicyclohexylpiperidin-4-yl)oxalamide (13b)

By use of a procedure similar to that described for the preparation of compound **8a**, the compound **6b** (31.3 mg, 0.120 mmol) was converted into the title compound **13b** (28.0 mg, 52% yield) as white powder.

^{1}H NMR (400 MHz, $CDCl_3$) δ 0.96 (t, J = 12.5 Hz, 2H), 1.10–1.84 (br, 20H), 2.05–2.19 (m, 2H), 4.08–4.21 (m, 1H), 7.23–7.33 (br, 1H), 7.39–7.46 (m, 2H), 7.88 (t, J = 1.00 Hz, 1H), 9.34 (s, 1H); ^{13}C NMR (125 MHz, $CDCl_3$) δ 14.1, 22.1 (2C), 22.7 (2C), 26.1 (2C), 31.6, 37.2 (2C), 42.6, 43.0, 43.6, 52.6 (2C), 119.0, 121.4, 128.7, 130.8, 133.1, 135.8, 157.7, 158.5; HRMS (ESI), m/z calcd for $C_{23}H_{32}Cl_2N_3O_2$ (MH^+) 452.1872, found 452.1865.

4.1.16. N^1-((4-Chloro-3-methylphenyl)-N^2-(2,6-dicyclohexylpiperidin-4-yl)oxalamide (13c)

By use of a procedure similar to that described for the preparation of compound **8a**, the compound **6c** (121.0 mg, 0.500 mmol) was converted into the title compound **13c** (15.1 mg, 7% yield) as white powder.

^{1}H NMR (500 MHz, $CDCl_3$) δ 0.87–1.88 (br, 22H), 2.09–2.20 (m, 2H), 2.38 (s, 3H), 4.09–4.22 (m, 1H), 7.32–7.33 (m, 1H), 7.41–7.43 (m, 1H), 7.51 (d, J = 2.00 Hz, 1H), 7.73 (m, 1H), 9.24 (s, 1H); ^{13}C NMR (125 MHz, $CDCl_3$) δ 20.2, 22.1 (2C), 22.7 (2C), 26.0 (2C), 29.7, 37.0, 42.3 (2C), 42.8 (2C), 43.4, 52.9 (2C), 118.4, 122.0, 130.0, 130.6, 134.8, 137.1, 157.5, 158.9; HRMS (ESI), m/z calcd for $C_{24}H_{35}ClN_3O_2$ (MH^+) 430.2267, found 430.2264.

4.1.17. N^1-(3-Fluoro-4-methylphenyl)-N^2-(2,6-dicyclohexylpiperidin-4-yl)oxalamide (14a)

By use of a procedure similar to that described for the preparation of compound **8a**, the compound **7a** (225.0 mg, 1.00 mmol) was converted into the title compound **14a** (27.5 mg, 7% yield) as white powder.

^{1}H NMR (500 MHz, $CDCl_3$) δ 0.971 (t, J = 12.5 Hz, 2H), 1.18–1.86 (m, 20H), 2.13–2.16 (m, 2H), 2.26 (s, 3H), 4.09–4.21 (m, 1H), 7.13–7.18 (m, 2H), 7.33 (d, J = 8.00 Hz, 1H), 7.50–7.53 (m, 1H), 9.27 (s, 1H); ^{13}C NMR (125 MHz, $CDCl_3$) δ 14.2, 22.2 (2C), 22.8 (2C), 26.1 (2C), 37.2 (2C), 42.2 (2C), 43.3 (2C), 43.5, 52.6 (m, 2C), 107.0 (d, J = 27.5 Hz), 115.0 (d, J = 3.75 Hz), 121.8 (d, J = 17.5 Hz), 131.6 (d, J = 6.25 Hz), 135.4 (d, J = 10.0 Hz), 157.5, 158.9, 161.3 (d, J = 242.5 Hz); HRMS (ESI), m/z calcd for $C_{24}H_{33}FN_3O_2$ (MH^-) 414.2554, found 414.2562.

4.1.18. N^1-(3-Chloro-4-methylphenyl)-N^2-(2,6-dicyclohexylpiperidin-4-yl)oxalamide (14b)

By use of a procedure similar to that described for the preparation of compound **8a**, the compound **7b** (120.5 mg, 0.500 mmol) was converted into the title compound **14b** (12.9 mg, 6% yield) as white powder.

^{1}H NMR (500 MHz, $CDCl_3$) δ 0.973 (t, J = 12.5 Hz, 2H), 1.18–1.86 (br, 20H), 2.11–2.19 (m, 2H), 2.35 (s, 3H), 4.09–4.21 (m, 1H), 7.20–7.22 (m, 1H), 7.30–7.32 (m, 1H), 7.35–7.37 (d, J = 2.50 Hz, 1H), 7.73 (m, 1H), 9.22 (s, 1H); ^{13}C NMR (125 MHz, $CDCl_3$) δ 19.6, 22.1 (2C), 22.7 (2C), 26.0 (2C), 29.7, 37.0, 42.1 (2C), 42.7 (2C), 43.2, 53.3 (2C), 118.0, 120.3, 131.2, 133.0, 134.7, 135.1, 157.5, 158.8; HRMS (ESI), m/z calcd for $C_{24}H_{33}ClN_3O_2$ (MH^+) 430.2267, found 430.2257.

4.1.19. N^1-(3-Bromo-4-methylphenyl)-N^2-(2,6-dicyclohexylpiperidin-4-yl)oxalamide (14c)

By use of a procedure similar to that described for the preparation of compound **8a**, the compound **7c** (142.0 mg, 0.500 mmol) was converted into the title compound **14c** (11.5 mg, 5% yield) as white powder.

^{1}H NMR (500 MHz, $CDCl_3$) δ 0.67–2.07 (br, 22H), 2.28 (br, 2H), 2.38 (s, 3H), 4.09–4.21 (m, 1H), 7.22 (d, J = 8.00 Hz, 1H), 7.28–7.38 (br, 1H), 7.43 (dd, J = 4.50, 2.50 Hz, 1H), 7.90 (d, J = 2.50 Hz, 1H), 9.21 (s, 1H); ^{13}C NMR (125 MHz, $CDCl_3$) δ 14.1, 22.1 (2C), 22.4 (2C), 22.7 (2C), 25.9, 30.0, 31.6, 36.9 (2C), 42.7 (3C), 52.7, 52.9, 118.6, 123.4, 125.0, 131.0, 134.9, 135.1, 157.4, 158.8; HRMS (ESI), m/z calcd for $C_{24}H_{33}BrN_3O_2$ (MH^+) 474.1762, found 474.1746.

4.2. Antiviral assay and cytotoxicity assay

Anti-HIV activity and cytotoxicity measurements in PM1/CCR5 cells (Yoshimura et al., 2010) were based on viability of cells that

had been infected or not infected with 100 TCID50 of an R5 primary isolate YTA48P exposed to various concentrations of the test compound. After the PM1/CCR5 cells were incubated at 37 °C for 7 days. The 50% inhibitory concentration (IC_{50}) values and the 50% cytotoxic concentration (CC_{50}) were then determined using the Cell Counting Kit-8 assay (Dojindo Laboratories). All assays were performed in duplicate or triplicate.

4.3. FACS analysis

JR-FL (R5, Sub B) chronically infected PM1 cells were pre-incubated with 0.5 μg/mL of sCD4 or 100 μM of a CD4 mimic for 15 min, and then incubated with an anti-HIV-1 mAb, 4C11, at 4 °C for 15 min. The cells were washed with PBS, and fluorescein isothiocyanate (FITC)-conjugated mouse anti-human IgG antibody was used for antibody-staining. Flow cytometry data for the binding of 4C11 (green lines) to the Env-expressing cell surface in the presence of a CD4 mimic are shown among gated PM1 cells along with a control antibody (anti-human CD19: black lines). Data are representative of the results from a minimum of two independent experiments. The number at the bottom of each graph shows the mean fluorescence intensity (MFI) of the antibody 4C11.

4.4. Molecular modeling

Dockings of compounds **3** and **13a** were performed using Molecular Operating Environment modeling package (MOE 2008. 10, Canada), into the crystal structure of gp120 (PDB, entry 3TGS).

Acknowledgements

This work was supported in part by Grant-in-Aid for Scientific Research from the Ministry of Education, Culture, Sports, Science, and Technology of Japan, and Health and Labour Sciences Research Grants from Japanese Ministry of Health, Labor, and Welfare. We are grateful to Professor Yoshio Hayashi and Dr. Fumika Yakushiji, Tokyo University of Pharmacy and Life Sciences for their assistance in the molecular modelings.

Supplementary data

Supplementary data (NMR charts of compounds) associated with this article can be found, in the online version, at http://dx.doi.org/10.1016/j.bmc.2013.02.041.

References and notes

1. Chan, D. C.; Kim, P. S. *Cell* **1998**, *93*, 681.
2. (a) Kadow, J.; Wang, H.-G.; Lin, P.-F. *Curr. Opin. Investig. Dugs* **2006**, *7*, 721; (b) Repik, A.; Clapham, P. R. *Structure* **2008**, *16*, 1603.
3. Holz-Smith, S.; Sun, I. C.; Jin, L.; Matthews, T. J.; Lee, K. H.; Chen, C. H. *Antimicrob. Agents Chemother.* **2001**, *45*, 60.
4. Lin, P.-F.; Blair, W.; Wang, T.; Spicer, T.; Guo, Q.; Zhou, N.; Gong, Y.-F.; Wang, H.-F. H.; Rose, R.; Yamanaka, G.; Robinson, B.; Li, C.-B.; Fridell, R.; Deminie, C.; Demers, G.; Yang, Z.; Zadjura, L.; Meanwell, N.; Colonno, R. *Proc. Natl. Acad. Sci. U.S.A.* **2003**, *100*, 11013.
5. Zhao, Q.; Ma, L.; Jiang, S.; Lu, H.; Liu, S.; He, Y.; Strick, N.; Neamati, N.; Debnath, A. K. *Virology* **2005**, *339*, 213.
6. (a) Madani, N.; Schön, A.; Princiotto, A. M.; LaLonde, J. M.; Courter, J. R.; Soeta, T.; Ng, D.; Wang, L.; Brower, E. T.; Xiang, S.-H.; Do Kwon, Y.; Huang, C.-C.; Wyatt, R.; Kwong, P. D.; Freire, E.; Smith, A. B., III; Sodroski, J. *Structure* **2008**, *16*, 1689; (b) LaLonde, J. M.; Elban, M. A.; Courter, J. R.; Sugawara, A.; Soeta, T.; Madani, N.; Princiotto, A. M.; Kwon, Y. D.; Kwong, P. D.; Schön, A.; Freire, E.; Sodroski, J.; Smith, A. B., III *Bioorg. Med. Chem. Lett.* **2011**, *20*, 354; (c) LaLonde, J. M.; Kwon, Y. D.; Jones, D. M.; Sun, A. W.; Courter, J. R.; Soeta, T.; Kobayashi, T.; Princiotto, A. M.; Wu, X.; Schön, A.; Freire, E.; Kwong, P. D.; Mascola, J. R.; Sodroski, J.; Madani, N.; Smith, A. B., III *J. Med. Chem.* **2012**, *55*, 4382.
7. Curreli, F.; Choudhury, S.; Pyatkin, I.; Zagorodnikov, V. P.; Bulay, A. K.; Altieri, A.; Kwon, Y. D.; Kwon, P. D.; Debnath, A. K. *J. Med. Chem.* **2012**, *55*, 4764.
8. (a) Yamada, Y.; Ochiai, C.; Yoshimura, K.; Tanaka, T.; Ohashi, N.; Narumi, T.; Nomura, W.; Harada, S.; Matsushita, S.; Tamamura, H. *Bioorg. Med. Chem. Lett.* **2010**, *20*, 354; (b) Narumi, T.; Ochiai, C.; Yoshimura, K.; Harada, S.; Tanaka, T.; Nomura, W.; Arai, H.; Ozaki, T.; Ohashi, N.; Matsushita, S.; Tamamura, H. *Bioorg. Med. Chem. Lett.* **2010**, *20*, 5853; (c) Narumi, T.; Arai, H.; Yoshimura, K.; Harada, S.; Nomura, W.; Matsushita, S.; Tamamura, H. *Bioorg. Med. Chem.* **2011**, *19*, 6735.
9. (a) Schön, A.; Madani, N.; Klein, J. C.; Hubicki, A.; Ng, D.; Yang, X.; Smith, A. B., III; Sodroski, J.; Freire, E. *Biochemistry* **2006**, *45*, 10973; (b) Schön, A.; Lam, S. Y.; Freire, E. *Future Med. Chem.* **2011**, *3*, 1129.
10. Yoshimura, K.; Harada, S.; Shibata, J.; Hatada, M.; Yamada, Y.; Ochiai, C.; Tamamura, H.; Matsushita, S. *J. Virol.* **2010**, *84*, 7558.
11. Kwon, Y. D.; Finzi, A.; Wu, X.; Dogo-Isonagie, C.; Lee, L. K.; Moore, L. R.; Schmidt, S. D.; Stuckey, J.; Yang, Y.; Zhou, T.; Zhu, J.; Vicic, D. A.; Debnath, A. K.; Shapiro, L.; Bewley, C. A.; Mascola, J. R.; Sodroski, J. G.; Kwong, P. D. *Proc. Natl. Acad. Sci. U.S.A.* **2012**, *109*, 5663.
12. (a) Kwong, P. D.; Wyatt, R.; Robinson, J.; Sweet, R. W.; Sodroski, J.; Hendrickson, W. A. *Nature* **1998**, *393*, 648; (b) Kwong, P. D.; Wyatt, R.; Mcajeed, S.; Robinson, J.; Sweet, R. W.; Sodroski, J.; Hendrickson, W. A. *Structure* **2000**, *8*, 1329.
13. McFarland, C.; Vicic, D. A.; Debnath, A. K. *Synthesis* **2006**, 807.
14. Sakai, K.; Yamada, K.; Yamasaki, T.; Kinoshita, Y.; Mito, F.; Utsumi, H. *Tetrahedron* **2010**, *66*, 2311.